

Implicit step-truncation integration of nonlinear PDEs on low-rank tensor manifolds

Abram Rodgers^a, Daniele Venturi^{a,*}

^a*Department of Applied Mathematics
University of California Santa Cruz, CA 95064*

Abstract

Explicit step-truncation tensor methods have recently proven successful in integrating initial value problems for high-dimensional partial differential equations (PDEs). However, the combination of non-linearity and stiffness may introduce time-step restrictions which could make explicit integration computationally infeasible. To overcome this problem, in this paper we develop a new class of implicit rank-adaptive algorithms for temporal integration of nonlinear evolution equations on tensor manifolds. These algorithms are based on performing one time step with a conventional time-stepping scheme, followed by an implicit fixed point iteration step involving a rank-adaptive truncation operation onto a tensor manifold. Implicit step truncation methods are straightforward to implement as they rely only on arithmetic operations between tensors, which can be performed by efficient and scalable parallel algorithms. Numerical applications demonstrating the effectiveness of implicit step-truncation tensor integrators are presented and discussed for the Allen-Cahn equation, the Fokker-Planck equation, and the nonlinear Schrödinger equation.

1. Introduction

High-dimensional nonlinear evolution equations of the form

$$\frac{\partial f(\mathbf{x}, t)}{\partial t} = \mathcal{N}(f(\mathbf{x}, t), \mathbf{x}), \quad f(\mathbf{x}, 0) = f_0(\mathbf{x}), \quad (1)$$

arise in many areas of mathematical physics, e.g., in statistical mechanics [7, 36], quantum field theory [47], and in the approximation of functional differential equations (infinite-dimensional PDEs) [45, 44] such as the Hopf equation of turbulence [26], or E's equation of deep learning [19]. In equation (1), $f : \Omega \times [0, T] \rightarrow \mathbb{R}$ is a d -dimensional (time-dependent) scalar field defined on the domain $\Omega \subseteq \mathbb{R}^d$ ($d \geq 2$), T is the period of integration, and \mathcal{N} is a nonlinear operator which may depend on the variables $\mathbf{x} = (x_1, \dots, x_d) \in \Omega$, and may incorporate boundary conditions. For simplicity, we assume that the domain Ω is a Cartesian product of d one-dimensional domains Ω_i

$$\Omega = \Omega_1 \times \dots \times \Omega_d, \quad (2)$$

*Corresponding author

Email addresses: `akrodger@ucsc.edu` (Abram Rodgers), `venturi@ucsc.edu` (Daniele Venturi)

and that f is an element of a Hilbert space $H(\Omega; [0, T])$. In these hypotheses, we can leverage the isomorphism $H(\Omega; [0, T]) \simeq H([0, T]) \otimes H(\Omega_1) \otimes \cdots \otimes H(\Omega_d)$ and represent the solution of (1) as

$$f(\mathbf{x}, t) \approx \sum_{i_1=1}^{n_1} \cdots \sum_{i_d=1}^{n_d} f_{i_1 \dots i_d}(t) \phi_{i_1}(x_1) \cdots \phi_{i_d}(x_d), \quad (3)$$

where $\phi_{i_j}(x_j)$ are one-dimensional orthonormal basis functions of $H(\Omega_j)$. Substituting (3) into (1) and projecting onto an appropriate finite-dimensional subspace of $H(\Omega)$ yields the semi-discrete form

$$\frac{d\mathbf{f}}{dt} = \mathbf{G}(\mathbf{f}), \quad \mathbf{f}(0) = \mathbf{f}_0 \quad (4)$$

where $\mathbf{f} : [0, T] \rightarrow \mathbb{R}^{n_1 \times n_2 \times \cdots \times n_d}$ is a multivariate array with coefficients $f_{i_1 \dots i_d}(t)$, and \mathbf{G} is the finite-dimensional representation of the nonlinear operator \mathcal{N} . The number of degrees of freedom associated with the solution to the Cauchy problem (4) is $N_{\text{dof}} = n_1 n_2 \cdots n_d$ at each time $t \geq 0$, which can be extremely large even for moderately small dimension d . For instance, the solution of the Boltzmann-BGK equation on a six-dimensional ($d = 6$) flat torus [9, 17] with $n_i = 256$ basis functions in each position and momentum variable yields $N_{\text{dof}} = 256^6 = 281474976710656$ degrees of freedom at each time t . This requires approximately 35.18 Terabytes per temporal snapshot if we store the solution tensor \mathbf{f} in a double precision IEEE 754 floating point format. Several general-purpose algorithms have been developed to mitigate such an exponential growth of degrees of freedom, the computational cost, and the memory requirements. These algorithms include, e.g., sparse collocation methods [10, 6, 20, 33], high-dimensional model representation (HDMR) [31, 11, 5], and techniques based on deep neural networks [34, 35, 46, 12].

In a parallel research effort that has its roots in quantum field theory and quantum entanglement, researchers have recently developed a new generation of efficient algorithms based on tensor networks and low-rank tensor techniques to compute the solution of high-dimensional PDEs [28, 4, 8, 13, 29]. Tensor networks are essentially factorizations of entangled objects such as multivariate functions or operators, into networks of simpler objects which are amenable to efficient representation and computation. The process of building a tensor network relies on a hierarchical decomposition that can be visualized in terms of trees, and has its roots in the spectral theory for linear operators. Such rigorous mathematical foundations opened the possibility to construct high-order methods to compute the numerical solution of high-dimensional Cauchy problems of the form (4) at a cost that scales linearly with respect to the dimension d , and polynomially with respect to the tensor rank.

In particular, a new class of algorithms to integrate (4) on a low-rank tensor manifold was recently proposed in [38, 16, 37, 15, 29, 44]. These algorithms are known as explicit step-truncation methods and they are based on integrating the solution $\mathbf{f}(t)$ off the tensor manifold for a short time using any conventional explicit time-stepping scheme, and then mapping it back onto the manifold using a tensor truncation operation (see Figure 2). To describe these methods further, let us discretize the ODE (4) in time with a one-step method on an evenly-spaced temporal grid as

$$\mathbf{f}_{k+1} = \Psi_{\Delta t}(\mathbf{G}, \mathbf{f}_k), \quad \mathbf{f}_0 = \mathbf{f}(0), \quad (5)$$

where \mathbf{f}_k denotes an approximation of $\mathbf{f}(k\Delta t)$ for $k = 0, 1, \dots$, and $\Psi_{\Delta t}$ is an increment function. To obtain a step-truncation integrator, we simply apply a truncation operator $\mathfrak{T}_{\mathbf{r}}(\cdot)$, i.e., a nonlinear projection onto a tensor manifold $\mathcal{H}_{\mathbf{r}}$ with multilinear rank \mathbf{r} [43] to the scheme (5). This yields

$$\mathbf{f}_{k+1} = \mathfrak{T}_{\mathbf{r}}(\Psi_{\Delta t}(\mathbf{G}, \mathbf{f}_k)). \quad (6)$$

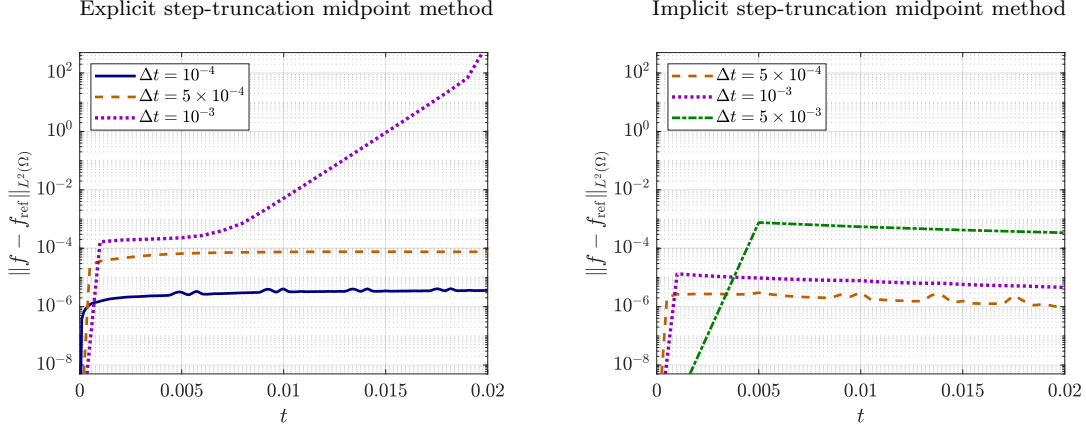


Figure 1: Explicit and implicit step-truncation midpoint methods applied the Allen-Cahn equation (7). It is seen that the explicit step-truncation midpoint method undergoes a numerical instability for $\Delta t = 10^{-3}$ while the implicit step-truncation midpoint method retains accuracy and stability for $\Delta t = 10^{-3}$, and even larger time steps.

The need for tensor rank-reduction when iterating (5) can be easily understood by noting that tensor operations such as the application of an operator to a tensor and the addition between two tensors naturally increase tensor rank [30]. Hence, iterating (6) with no rank reduction can yield a fast increase in tensor rank, which, in turn, can tax computational resources heavily.

Explicit step-truncation algorithms of the form (6) were studied extensively in [37, 29]. In particular, error estimates and convergence results were obtained for both fixed-rank and rank-adaptive integrators, i.e., integrators in which the tensor rank \mathbf{r} is selected at each time step based on accuracy and stability constraints. Step-truncation methods are very simple to implement as they rely only on arithmetic operations between tensors, which can be performed by scalable parallel algorithms [14, 40, 3, 22].

While explicit step-truncation methods have proven successful in integrating a wide variety of high-dimensional initial value problems, their effectiveness for *stiff problems* is limited. Indeed, the combination of non-linearity and stiffness may introduce time-step restrictions which could make explicit step-truncation integration computationally infeasible. As an example, in Figure 1 we show that the explicit step-truncation midpoint method applied to the Allen-Cahn equation

$$\frac{\partial f}{\partial t} = \varepsilon \Delta f + f - f^3, \quad (7)$$

undergoes a numerical instability for $\Delta t = 10^{-3}$.

The main objective of this paper is to develop a new class of rank-adaptive *implicit* step-truncation algorithms to integrate high-dimensional initial value problems of the form (4) on tensor manifolds. The main idea of these new integrators is illustrated in Figure 2. Roughly speaking, implicit step-truncation method take $\mathbf{f}_k \in \mathcal{H}_{\mathbf{r}}$ and $\Psi_{\Delta t}(\mathbf{G}, \mathbf{f}_k)$ as input and generate a sequence of fixed-point iterates $\mathbf{f}^{[j]}$ converging to a point tensor manifold $\mathcal{H}_{\mathbf{s}}$. Once $\mathbf{f}^{[j]}$ is sufficiently close to $\mathcal{H}_{\mathbf{s}}$ we project it onto the manifold. Of course the computational cost of implicit step-truncation methods is higher than explicit step truncation methods at each step. However, implicit methods allow to integrate stably with larger time-steps while retaining accuracy (see Figure 1).

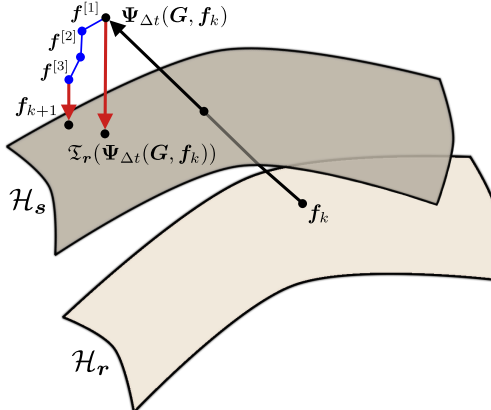


Figure 2: Sketch of implicit and explicit step-truncation integration methods. Given a tensor \mathbf{f}_k with multilinear rank \mathbf{r} on the manifold \mathcal{H}_r , we first perform an explicit time-step, e.g., with the conventional time-stepping scheme (5). The explicit step-truncation integrator then projects $\Psi_{\Delta t}(\mathbf{G}, \mathbf{f}_k)$ onto a new tensor manifold \mathcal{H}_s (projection illustrated with a solid red line). The multilinear rank \mathbf{s} is chosen adaptively based on desired accuracy and stability constraints [37]. On the other hand, the implicit step-truncation method takes $\Psi_{\Delta t}(\mathbf{G}, \mathbf{f}_k)$ as input and generates a sequence of fixed-point iterates $\mathbf{f}^{[j]}$ shown as dots connected with blue lines. The last iterate is then projected onto a low rank tensor manifold, illustrated here also as a red line landing on \mathcal{H}_s .

Previous research on implicit tensor integration leveraged the Alternating Least Squares (ALS) algorithm [8, 18, 13], which essentially attempts to solve an optimization problem on a low-rank tensor manifold to compute the solution of (4) at each time step. As is well-known, ALS is equivalent to the (linear) block Gauss-Seidel iteration applied to the Hessian matrix of the residual, and can have convergence issues [42].

The paper is organized as follows. In section 2, we briefly review rank-adaptive explicit step-truncation methods, and present a new convergence proof for these methods which applies also to implicit step-truncation methods. In section 3, we discuss the proposed new algorithms for implicit step-truncation integration. In section 4 and section 5 we study convergence of particular implicit step-truncation methods, namely the step-truncation implicit Euler and midpoint methods, respectively. Finally, in section 7 we present numerical applications of implicit step-truncation algorithms to stiff PDEs. In particular, we study a two-dimensional Allen-Cahn equation, a four-dimensional Fokker-Planck equation, and six-dimensional nonlinear Schrödinger equation.. We also include two appendices providing the convergence proof of implicit rank-adaptive fixed point iterations, and an outline how to develop high-order implicit multi-step integration methods using the implicit step-truncation framework we propose.

2. Explicit step-truncation methods

In this section we briefly review explicit step-truncation methods to integrate the tensor-valued ODE (4) on tensor manifolds with variable rank. For a complete account of this theory see [37]. We begin by first discretizing the ODE in time with any standard one-step method on an evenly-spaced temporal grid

$$\mathbf{f}_{k+1} = \Psi_{\Delta t}(\mathbf{G}, \mathbf{f}_k). \quad (8)$$

Here, \mathbf{f}_k denotes an approximation of the exact solution $\mathbf{f}(k\Delta t)$ for $k = 1, 2, \dots$, and $\Psi_{\Delta t}$ is an increment function. For example, $\Psi_{\Delta t}$ can be the increment function defining the Euler forward method

$$\Psi_{\Delta t}(\mathbf{G}, \mathbf{f}_k) = \mathbf{f}_k + \Delta t \mathbf{G}(\mathbf{f}_k). \quad (9)$$

In the interest of saving computational resources when iterating (8) we look for an approximation of \mathbf{f}_k on a low-rank tensor manifold \mathcal{H}_r [43] with multilinear rank \mathbf{r} . The easiest way for approximating (8) on \mathcal{H}_r is to apply a nonlinear projection operator [21] (truncation operator)

$$\mathfrak{T}_r : \mathbb{R}^{n_1 \times n_2 \times \dots \times n_d} \rightarrow \overline{\mathcal{H}_r}, \quad (10)$$

where $\overline{\mathcal{H}_r}$ denotes the closure of \mathcal{H}_r . This yields the explicit step-truncation scheme

$$\mathbf{f}_{k+1} = \mathfrak{T}_r(\Psi_{\Delta t}(\mathbf{G}, \mathbf{f}_k)). \quad (11)$$

The rank \mathbf{r} can be chosen with every time step based on appropriate error estimates as time integration proceeds [37]. We can also project $\mathbf{G}(\mathbf{f})$ onto $\overline{\mathcal{H}_r}$ before applying $\Psi_{\Delta t}$. With reference to (9) this yields

$$\mathbf{f}_{k+1} = \mathfrak{T}_{r_2}(\mathbf{f}_k + \Delta t \mathfrak{T}_{r_1}(\mathbf{G}(\mathbf{f}_k))). \quad (12)$$

Here \mathbf{r}_1 and \mathbf{r}_2 are truncation ranks determined by the inequalities¹

$$\|\mathbf{G}(\mathbf{f}_k) - \mathfrak{T}_{r_1}(\mathbf{G}(\mathbf{f}_k))\| \leq e_1 \quad \left\| \tilde{\mathbf{f}}_{k+1} - \mathfrak{T}_{r_2}(\tilde{\mathbf{f}}_{k+1}) \right\| \leq e_2, \quad (13)$$

where e_1 and e_2 are chosen error thresholds. As before, \mathbf{r}_1 and \mathbf{r}_2 can change with every time step. It was recently shown in [37] that if we choose $e_1 = K_1 \Delta t$ and $e_2 = K_2 \Delta t^2$ (with K_1 and K_2 given constants) then the step-truncation method (12) is convergent. More generally, let

$$\mathbf{f}_{k+1} = \Phi_{\Delta t}(\mathbf{G}, \mathbf{f}_k, \mathbf{e}) \quad (14)$$

be a step-truncation method in which all we project all $\mathbf{G}(\mathbf{f}_k)$ appearing in the increment function $\Psi_{\Delta t}(\mathbf{G}, \mathbf{f}_k)$ onto tensor manifolds $\overline{\mathcal{H}_{r_i}}$ by setting suitable error thresholds e_i . For instance, if $\Psi_{\Delta t}$ is defined by the midpoint method, i.e.,

$$\Psi_{\Delta t}(\mathbf{G}, \mathbf{f}_k) = \mathbf{f}_k + \mathbf{G}\left(\mathbf{f}_k + \frac{\Delta t}{2} \mathbf{G}(\mathbf{f}_k)\right) \quad (15)$$

then

$$\Phi_{\Delta t}(\mathbf{G}, \mathbf{f}_k, \mathbf{e}) = \mathfrak{T}_{r_3}\left(\mathbf{f}_k + \mathfrak{T}_{r_2}\left[\mathbf{G}\left(\mathbf{f}_k + \frac{\Delta t}{2} \mathfrak{T}_{r_1}[\mathbf{G}(\mathbf{f}_k)]\right)\right]\right) \quad (16)$$

where $\mathbf{e} = (e_1, e_2, e_3)$ is a vector collecting the truncation error thresholds yielding the multilinear ranks \mathbf{r}_1 , \mathbf{r}_2 and \mathbf{r}_3 . By construction, step-truncation methods of the form (14) satisfy

$$\|\Psi_{\Delta t}(\mathbf{G}, \mathbf{f}) - \Phi_{\Delta t}(\mathbf{G}, \mathbf{f}, \mathbf{e})\| \leq R(\mathbf{e}), \quad (17)$$

where $R(\mathbf{e})$ is the total error due to tensor truncation. We close this section with a reformulation of the convergence theorem for explicit step-truncation methods in [37] which applies also to implicit methods.

¹Throughout the paper $\|\cdot\|$ denotes the standard tensor 2-norm [21, 30], or a weighted version of it.

Theorem 2.1 (Convergence of step-truncation methods). *Let $\varphi_{\Delta t}(\mathbf{G}, \mathbf{f})$ be the one-step exact flow map defined by (4), and $\Phi_{\Delta t}(\mathbf{G}, \mathbf{f}, \mathbf{e})$ be the increment function of a step-truncation method with local error of order p , i.e.,*

$$\|\varphi_{\Delta t}(\mathbf{G}, \mathbf{f}) - \Phi_{\Delta t}(\mathbf{G}, \mathbf{f}, \mathbf{e})\| \leq K\Delta t^{p+1} \quad \text{as } \Delta t \rightarrow 0. \quad (18)$$

If there exist truncation errors $\mathbf{e} = \mathbf{e}(\Delta t)$ (function of Δt) so that the stability condition

$$\left\| \Phi_{\Delta t}(\mathbf{G}, \hat{\mathbf{f}}, \mathbf{e}) - \Phi_{\Delta t}(\mathbf{G}, \tilde{\mathbf{f}}, \mathbf{e}) \right\| \leq (1 + C\Delta t) \left\| \hat{\mathbf{f}} - \tilde{\mathbf{f}} \right\| + E\Delta t^{m+1} \quad (19)$$

holds as $\Delta t \rightarrow 0$, then the step-truncation method is convergent with order $z = \min(m, p)$.

Proof. Under the assumption that Δt is small enough for our stability and consistency to hold, we proceed by induction. The $k = 1$ case coincides with the consistency condition. Next, we assume the that

$$\|\varphi_{\Delta t(N-1)}(\mathbf{G}, \mathbf{f}_0) - \mathbf{f}_{N-1}\| \leq Q_{N-1}\Delta t^z. \quad (20)$$

Let $T = N\Delta t$ be the final integration time. By applying triangle inequality and the semigroup property of the flow map,

$$\begin{aligned} \|\varphi_T(\mathbf{G}, \mathbf{f}_0) - \Phi_{\Delta t}(\mathbf{G}, \mathbf{f}_{N-1}, \mathbf{e})\| &\leq \|\varphi_{\Delta t}(\mathbf{G}, \varphi_{\Delta t(N-1)}(\mathbf{G}, \mathbf{f}_0)) - \Phi_{\Delta t}(\mathbf{G}, \varphi_{\Delta t(N-1)}(\mathbf{G}, \mathbf{f}_0), \mathbf{e})\| \\ &\quad + \|\Phi_{\Delta t}(\mathbf{G}, \varphi_{\Delta t(N-1)}(\mathbf{G}, \mathbf{f}_0), \mathbf{e}) - \Phi_{\Delta t}(\mathbf{G}, \mathbf{f}_{N-1}, \mathbf{e})\|. \end{aligned} \quad (21)$$

By consistency (18), the first term at the right hand side can be bounded by $K_{N-1}\Delta t^{p+1}$, where each K_j represents a local error coefficient. Using the stability condition (19), we can bound the second term as

$$\|\Phi_{\Delta t}(\mathbf{G}, \varphi_{\Delta t(N-1)}(\mathbf{G}, \mathbf{f}_0), \mathbf{e}) - \Phi_{\Delta t}(\mathbf{G}, \mathbf{f}_{N-1}, \mathbf{e})\| \leq (1 + C\Delta t) \|\varphi_{\Delta t(N-1)}(\mathbf{G}, \mathbf{f}_0) - \mathbf{f}_{N-1}\| + E\Delta t^{m+1}. \quad (22)$$

A substitution of (22) and (20) into (21) yields

$$\|\varphi_T(\mathbf{G}, \mathbf{f}_0) - \Phi_{\Delta t}(\mathbf{G}, \mathbf{f}_{N-1}, \mathbf{e})\| \leq K_{N-1}\Delta t^{p+1} + (1 + C\Delta t)Q_{N-1}\Delta t^z + E\Delta t^{m+1}.$$

Recalling that $z = \min(m, p)$ completes the proof. □

We remark that the above proof may be modified to include step-truncation explicit multi-step methods, i.e., step-truncation Adams methods. To this end, it is sufficient to replace \mathbf{f}_k with the vector $(\mathbf{f}_{k-s}, \mathbf{f}_{k-s+1}, \dots, \mathbf{f}_k)$ and the stability condition (19) with

$$\left\| \Phi_{\Delta t}(\mathbf{G}, \hat{\mathbf{f}}_1, \hat{\mathbf{f}}_2, \dots, \hat{\mathbf{f}}_s, \mathbf{e}) - \Phi_{\Delta t}(\mathbf{G}, \tilde{\mathbf{f}}_1, \tilde{\mathbf{f}}_2, \dots, \tilde{\mathbf{f}}_s, \mathbf{e}) \right\| \leq \left\| \hat{\mathbf{f}}_1 - \tilde{\mathbf{f}}_1 \right\| + \sum_{j=1}^s C_j \Delta t \left\| \hat{\mathbf{f}}_j - \tilde{\mathbf{f}}_j \right\| + E\Delta t^{m+1}. \quad (23)$$

We then have an analogous theorem proven using an inductive argument based on the initial conditions $\mathbf{f}(0), \mathbf{f}(\Delta t), \dots, \mathbf{f}((s-1)\Delta t)$.

3. Implicit step-truncation methods

To introduce implicit step-truncation tensor methods, let us consider the conventional Euler backward scheme

$$\mathbf{f}_{k+1} = \mathbf{f}_k + \Delta t \mathbf{G}(\mathbf{f}_{k+1}), \quad (24)$$

and the associated root-finding problem

$$\mathbf{H}(\mathbf{f}_{k+1}) = \mathbf{f}_{k+1} - \mathbf{f}_k - \Delta t \mathbf{G}(\mathbf{f}_{k+1}) = \mathbf{0}. \quad (25)$$

Equation (25) allows us to compute \mathbf{f}_{k+1} as a zero of the function \mathbf{H} . This can be done, e.g., using the Newton's method with the initial guess $\mathbf{f}_{k+1}^{[0]} = \mathbf{f}_k$. As is well-known, if the Jacobian of \mathbf{H} is invertible within a neighborhood of \mathbf{f}_k , then the implicit function theorem guarantees the existence of a locally differentiable (in some neighborhood of \mathbf{f}_k) nonlinear map $\Theta_{\Delta t}$ depending on \mathbf{G} such that

$$\mathbf{f}_{k+1} = \Theta_{\Delta t}(\mathbf{G}, \mathbf{f}_k). \quad (26)$$

In the Newton's setting described above, the map $\Theta_{\Delta t}$ is computed iteratively. Then an implicit step-truncation scheme can be formulated by applying the tensor truncation operator \mathfrak{T}_r to the right hand side of (26), i.e.,

$$\mathbf{f}_{k+1} = \mathfrak{T}_r(\Theta_{\Delta t}(\mathbf{G}, \mathbf{f}_k)). \quad (27)$$

The tensor truncation rank r can be selected based on the inequality

$$\|\mathfrak{T}_r(\Theta_{\Delta t}(\mathbf{G}, \mathbf{f}_k)) - \Theta_{\Delta t}(\mathbf{G}, \mathbf{f}_k)\| \leq A \Delta t^2. \quad (28)$$

It was shown in [37] that this yields an order one (in time) integration scheme.

Of course, if the Jacobian of \mathbf{H} in equation (25) can be computed explicitly and stored in computer memory, then we can easily determine $\mathbf{f}_{k+1} = \Theta_{\Delta t}(\mathbf{G}, \mathbf{f}_k)$ for any given \mathbf{f}_k and \mathbf{G} , e.g., by using Newton's iterations. Unfortunately, for problems in which \mathbf{f}_k and \mathbf{f}_{k+1} are represented in a low-rank tensor format (or more generally for high-dimensional problems) it is not straightforward to compute the Jacobian of \mathbf{H} , and therefore compute the mapping $\Theta_{\Delta t}(\mathbf{G}, \mathbf{f}_k)$. However, we can approximate $\Theta_{\Delta t}(\mathbf{G}, \mathbf{f}_k)$ using the theory of *contraction mappings*. To this end, let us define the following iteration function associated with the Euler's backward method

$$\mathbf{Q}_k(\mathbf{f}) = \mathbf{f}_k + \Delta t \mathbf{G}(\mathbf{f}). \quad (29)$$

Since \mathbf{G} is Lipschitz continuous with Lipschitz constant L_G on some closed convex set $\mathcal{D} \subseteq \mathbb{R}^{n_1 \times \dots \times n_d}$ including \mathbf{f}_k we have that (29) satisfies

$$\|\mathbf{Q}_k(\mathbf{f}) - \mathbf{Q}_k(\mathbf{g})\| \leq \Delta t L_G \|\mathbf{f} - \mathbf{g}\|, \quad \text{for all } \mathbf{f}, \mathbf{g} \in \mathcal{D}. \quad (30)$$

Clearly, if

$$\Delta t < \frac{1}{L_G} \quad (31)$$

then \mathbf{Q}_k a (strict) contraction on \mathcal{D} . This implies that the fixed point iterates

$$\mathbf{f}^{[j+1]} = \mathbf{Q}_k(\mathbf{f}^{[j]}) \quad j = 0, 1, \dots \quad (32)$$

converge to the unique zero $\mathbf{f}_{k+1} \in \mathcal{D}$ satisfying $\mathbf{f}_{k+1} = \mathbf{Q}_k(\mathbf{f}_{k+1})$ for every² initial guess $\mathbf{f}^{[0]} \in \mathcal{D}$. Equation (31) can be seen as a stability condition restricting the maximum allowable Δt for the implicit Euler method with fixed point iterations.

More generally, let \mathbf{Q}_k be the mapping associated with an arbitrary implicit time integration scheme. For instance, \mathbf{Q}_k could be the mapping defined by the implicit midpoint rule

$$\mathbf{Q}_k(\mathbf{f}) = \mathbf{f}_k + \Delta t \mathbf{G} \left(\frac{\mathbf{f}_k + \mathbf{f}}{2} \right). \quad (33)$$

Representing $\mathbf{Q}_k(\mathbf{f})$ in a low-rank tensor format yields an approximated map $\tilde{\mathbf{Q}}_k(\mathbf{f})$. As before, there is no unique way to construct $\tilde{\mathbf{Q}}_k(\mathbf{f})$. For example, with reference to the implicit Euler mapping (29), one can define

$$\tilde{\mathbf{Q}}_k(\mathbf{f}) = \mathfrak{T}_{\mathbf{r}}(\mathbf{f}_k + \Delta t \mathbf{G}(\mathbf{f})) \quad (34)$$

or

$$\tilde{\mathbf{Q}}_k(\mathbf{f}) = \mathfrak{T}_{\mathbf{r}_2}(\mathbf{f}_k + \Delta t \mathfrak{T}_{\mathbf{r}_1}(\mathbf{G}(\mathbf{f}))), \quad (35)$$

where $\mathfrak{T}_{\mathbf{r}_1}$ and $\mathfrak{T}_{\mathbf{r}_2}$ are two tensor truncations with ranks \mathbf{r}_1 and \mathbf{r}_2 , respectively.

A fundamental question at this point is whether it possible to accurately approximate the sequence (32), by using fixed point iterations of $\tilde{\mathbf{Q}}_k(\mathbf{f})$, i.e., a tensor approximation of $\mathbf{Q}_k(\mathbf{f})$. The following theorem addresses this question and provides a constructive method with guaranteed convergence certificates to approximate the fixed point of (32) by a sequence of tensors. The theorem represents one of the main results of our paper and its proof is given in [Appendix A](#).

Theorem 3.1 (Convergence of rank-adaptive fixed point iterations). *Let \mathbf{Q}_k be a locally Lipschitz mapping associated with an implicit time integration scheme, $\mathcal{D} \subseteq \mathbb{R}^{n_1 \times \dots \times n_d}$ a closed convex set so that $\mathbf{Q}_k(\mathcal{D}) \subseteq \mathcal{D}$. For any $\varepsilon \geq 0$, let $\tilde{\mathbf{Q}}_k : \mathcal{D} \rightarrow \mathcal{D}$ be a map³ satisfying $\|\tilde{\mathbf{Q}}_k(\mathbf{f}) - \mathbf{Q}_k(\mathbf{f})\| \leq \varepsilon$ for all $\mathbf{f} \in \mathcal{D}$. If $q \in [0, 1)$ is a Lipschitz constant for \mathbf{Q}_k within \mathcal{D} and \mathbf{f}_{k+1} is the (unique) fixed point of \mathbf{Q}_k in \mathcal{D} , then the sequence $\mathbf{f}^{[j]}$ ($j = 0, 1, \dots$) defined as*

$$\mathbf{y}^{[j+1]} = \mathbf{Q}_k(\mathbf{f}^{[j]}), \quad (36)$$

$$\varepsilon_j = c \frac{1-q}{1+q} \|\mathbf{y}^{[j+1]} - \mathbf{f}^{[j]}\|, \quad (37)$$

$$\mathbf{f}^{[j+1]} = \tilde{\mathbf{Q}}_k(\mathbf{f}^{[j]}), \quad (38)$$

converges to \mathbf{f}_{k+1} for any choice of $\mathbf{f}^{[0]} \in \mathcal{D}$ and an arbitrary scalar $c \in (0, 1)$.

Let us briefly discuss how Theorem 3.1 relates to implicit step-truncation tensor methods. To this end, suppose we are given a tensor \mathbf{f}_k representing the solution to an ODE at time t_k and suppose we would like to compute a tensor approximation of the solution at time t_{k+1} . Theorem 3.1 is saying that the sequence of tensors (38) converges to \mathbf{f}_{k+1} , provided the mapping \mathbf{Q}_k is a contraction. Note that the truncation threshold (37) is iteration-dependent, and it may become smaller and smaller as j increases, yielding a rank-increase. The key steps of Theorem 3.1 are summarized in Algorithm 1 and in Figure 2. A useful corollary of Theorem 3.1 is the convergence rate of the fixed-point iterations.

²Recall that strict contraction on a complete metric space \mathcal{D} has a unique fixed point in \mathcal{D} .

³Note that $\tilde{\mathbf{Q}}_k$ depends on ε . This implies that the truncation rank will be larger when ε is smaller.

Algorithm 1: Rank-Adaptive Fixed Point Iterations

Input:

- $\mathbf{Q}_k : \mathcal{D} \rightarrow \mathcal{D}$ (contraction mapping on $\mathcal{D} \subseteq \mathbb{R}^{n_1 \times \dots \times n_d}$.)
- $\tilde{\mathbf{Q}}_k : \mathcal{D} \rightarrow \mathcal{D}$ (tensor approximation of \mathbf{Q}_k such that $\|\mathbf{Q}_k - \tilde{\mathbf{Q}}_k\| \leq \varepsilon$.)
- $\hat{q} \in (0, 1)$ (estimate for the Lipschitz constant of \mathbf{Q}_k .)
- $b \in [2, \infty)$ (proportionality constant for low rank compression error.)
- $\mathbf{f}^{[0]} \in \mathcal{D}$ (initial guess for the fixed point of \mathbf{Q}_k .)
- $\varepsilon_{\text{tol}} > 0$ (stopping tolerance of the fixed point iterations.)

Output: A tensor $\mathbf{f}^* \in \mathcal{D}$ such that $\|\mathbf{Q}_k(\mathbf{f}^*) - \mathbf{f}^*\| \leq \varepsilon_{\text{tol}}$
 (\mathbf{f}^* is an approximation of the fixed point \mathbf{f}_{k+1} .)

Runtime:

- while** $e_{j+1} \leq \varepsilon_{\text{tol}}$ **do:**
- $\mathbf{y}^{[j+1]} = \mathbf{Q}_k(\mathbf{f}^{[j]})$ Compute one iterate using the contraction mapping \mathbf{Q}_k .
- $e_{j+1} = \|\mathbf{y}^{[j+1]} - \mathbf{f}^{[j]}\|$ Compute the error for the fixed point estimate.
- $\varepsilon_{j+1} = e_{j+1} 2(1 - \hat{q})/b^2$ Compute the approximation error for $\tilde{\mathbf{Q}}_k$.
- $\mathbf{f}^{[j+1]} = \tilde{\mathbf{Q}}_k(\mathbf{f}^{[j]})$ Compute a new tensor with approximation error ε_{j+1} .

Return: $\mathbf{f}^* = \mathbf{f}^{[j+1]}$.

Theorem 3.2 (Convergence rate of fixed point iterations). *Let \mathbf{f}_{k+1} be the unique fixed point of \mathbf{Q}_k . Then the iterates $\mathbf{f}^{[j]}$ defined in Theorem 3.1 satisfy the error estimates*

$$\|\mathbf{f}_{k+1} - \mathbf{f}^{[j]}\| \leq \frac{g_c(q)^j}{1 - g_c(q)} \left(c \frac{1 - q}{1 + q} + 1 \right) \|\mathbf{Q}_k(\mathbf{f}^{[0]}) - \mathbf{f}^{[0]}\|, \quad (39)$$

$$\|\mathbf{f}_{k+1} - \mathbf{f}^{[j+1]}\| \leq \frac{g_c(q)}{1 - g_c(q)} \left(c \frac{1 - q}{1 + q} + 1 \right) \|\mathbf{Q}_k(\mathbf{f}^{[j]}) - \mathbf{f}^{[j]}\|, \quad (40)$$

where $g_c(q) = c(1 - q) + q$.

The proof follows immediately from one of the inequalities used to prove Theorem 3.1 (see [Appendix A](#)). The coefficient multiplying the norm at the right hand side of (40) appears quite frequently the forthcoming analysis, and therefore it is convenient to define it as

$$G_c(q) = \frac{g_c(q)}{1 - g_c(q)} \left(c \frac{1 - q}{1 + q} + 1 \right). \quad (41)$$

In practice, the exact value of the fixed point \mathbf{f}_{k+1} is not available. As with a standard approximation by fixed point iterations, we check when $\|\mathbf{Q}_k(\mathbf{f}^{[j+1]}) - \mathbf{f}^{[j+1]}\| \leq \varepsilon_{\text{tol}}$ (residual check) and use $\mathbf{f}^{[j+1]}$ as approximation of \mathbf{f}_{k+1} .

Note that the Lipschitz constant q comes up quite frequently in the results above. However, we need not use the smallest possible value of q in equation (37). Instead, we may replace $(1 - q)/(1 + q)$ with the lower bound $(1 - \hat{q})/b$ where $b \geq 2$ and $q \leq \hat{q} < 1$ without modifying any of the subsequent estimates. If this is done, then the parameter c has an optimized lower bound as $c_{\min} = 2/b$. In our numerical experiments (see section 7) we have found empirically that $b = 5$ works well.

Therefore, if we can provide a (problem-dependent) estimate for \hat{q} , then we can use the convergence rate corollary above to terminate the fixed point iterations, instead of checking the residual. The simplifications stated here are included in the description of Algorithm 1.

3.1. Implicit step-truncation update

While increasing the rank is necessary for convergence, it is possible that we raise the rank by more than is required in a single time step. Therefore, it is convenient to perform an additional truncation after computing $\mathbf{f}_{k+1}^{[j]}$. This gives us

$$\mathbf{f}_{k+1} = \mathfrak{T}_r \left(\mathbf{f}_{k+1}^{[j]} \right), \quad \left\| \mathfrak{T}_r \left(\mathbf{f}_{k+1}^{[j]} \right) - \mathbf{f}_{k+1}^{[j]} \right\| \leq e_r \quad (42)$$

We could select the truncation threshold e_r based on the singular value decay rate, as shown in [37]. This would ignore the extent to which the rank-adaptive fixed point iteration algorithm is overestimating rank. We can quantify this in order to select e_r . To this end, recall that the fixed point estimate $\mathbf{f}_{k+1}^{[j]}$ satisfies the local consistency condition

$$\left\| \mathbf{f}_{k+1}^{[j]} - \mathbf{f}((k+1)\Delta t) \right\| \leq (K_1 + G_c(q)B)\Delta t^{p+1}, \quad (43)$$

with $B = 1/G_c(0)$ (G_c is defined in (41)). By noting the error $\mathbf{E}_{k+1}^{[j]} = \mathbf{f}_{k+1}^{[j]} - \mathbf{f}((k+1)\Delta t)$ and rearranging we find

$$\mathbf{f}_{k+1}^{[j]} = \mathbf{f}((k+1)\Delta t) + \mathbf{E}_{k+1}^{[j]}. \quad (44)$$

Hence, if $\mathbf{f}((k+1)\Delta t)$ can be approximated well with a low rank tensor and $\mathbf{E}_{k+1}^{[j]}$ has any singular vectors independent of those for $\mathbf{f}((k+1)\Delta t)$, then $\mathbf{f}_{k+1}^{[j]}$ would overestimate the rank without any additional accuracy. Thus, if we can estimate $\left\| \mathbf{E}_{k+1}^{[j]} \right\|$ we may further compress the numerical approximation of the next time step. The singular values of $\mathbf{E}_{k+1}^{[j]}$ are of the order of the local error at the right side of (43). Therefore, we just need to estimate such local error and then apply an additional truncation after applying Algorithm 1. This can be accomplished in the following manner. Suppose $\Psi_{\Delta t}(\mathbf{G}, \mathbf{f})$ is an explicit integrator at least of the same order as the implicit method under consideration. Then we can estimate the local error as

$$\begin{aligned} \left\| \mathbf{f}_{k+1}^{[j]} - \mathbf{f}((k+1)\Delta t) \right\| &\leq \left\| \mathbf{f}_{k+1}^{[j]} - \Psi_{\Delta t}(\mathbf{G}, \mathbf{f}_k) \right\| + \left\| \Psi_{\Delta t}(\mathbf{G}, \mathbf{f}_k) - \mathbf{f}((k+1)\Delta t) \right\| \\ &= \left\| \mathbf{f}_{k+1}^{[j]} - \Psi_{\Delta t}(\mathbf{G}, \mathbf{f}_k) \right\| + O(\Delta t^{p+1}), \end{aligned} \quad (45)$$

Thus, we may roughly estimate the local truncation error and set this as the chosen error for approximation to HT or TT rank r using the threshold

$$e_r = \left\| \mathbf{f}_{k+1}^{[j]} - \Psi_{\Delta t}(\mathbf{G}, \mathbf{f}_k) \right\|. \quad (46)$$

We may drop more singular values than needed. However, this estimate guarantees that we do not change the overall convergence rate. Moreover, it cannot impact stability since the truncation operator has operator norm of 1 regardless of the rank chosen. In all numerical experiments performed in this paper we use the explicit step-truncation midpoint method to estimate the local error (46). The procedure for rank-adaptive implicit step-truncation tensor integration is described in Algorithm 2 for implicit schemes defined by arbitrary iteration functions \mathbf{Q}_k .

Algorithm 2: Implicit Step-Truncation Update

Input:
 $\mathbf{f}_k \in \mathcal{D} \subseteq \mathbb{R}^{n_1 \times \dots \times n_d}$ (tensor representing the state of the system at time t_k).

 $\mathbf{G} : \mathcal{D} \rightarrow \mathcal{D}$ (right hand side of (4)).

 $\Delta t > 0$ (time step).

 $\varepsilon_{\text{tol}} > 0$ (stopping tolerance for the implicit solver).

Output:
 \mathbf{f}_{k+1} , tensor solution solution at time t_{k+1} .

Runtime:

 Define the contraction mapping \mathbf{Q}_k associated with the implicit scheme

 Define a tensor approximation $\tilde{\mathbf{Q}}_k$ of the contraction mapping \mathbf{Q}_k

 Fix an upper bound Lipschitz constant $0 < \hat{q} < 1$, e.g. $\hat{q} = 0.9$.

 Apply Algorithm 1 to compute $\mathbf{f}_{k+1}^{[j]}$ (terminate iterations when tolerance is met)

 Compute an estimate \mathbf{v}_{k+1} of $\mathbf{f}((k+1)\Delta t)$ using an explicit method of the same order as \mathbf{Q}_k or higher.

 Set absolute error singular value tolerance $\varepsilon_{\text{trunc}} = \|\mathbf{v}_{k+1} - \mathbf{f}_{k+1}^{[j]}\|$.

 Compute $\mathbf{f}_{k+1} = \mathfrak{T}_{\mathbf{r}}(\mathbf{f}_{k+1}^{[j]})$ with absolute error tolerance $\varepsilon_{\text{trunc}}$.

Return: \mathbf{f}_{k+1} .

4. Implicit step-truncation Euler method

The conventional implicit Euler method to integrate (4) is

$$\mathbf{f}_{k+1} = \mathbf{f}_k + \Delta t \mathbf{G}(\mathbf{f}_{k+1}) \quad (47)$$

This method is well-known to be convergent with order one, and to have stability region $\{z \in \mathbb{C} : |z - 1| > 1\}$. The implicit step-truncation version of (47) is based on Theorem 3.1, in which the number of iterations of the algorithm is defined by the tolerance ε_{tol} such that $\|\mathbf{Q}_k(\mathbf{f}^{[j]}) - \mathbf{f}^{[j]}\| \leq \varepsilon_{\text{tol}}$. Let us now write down the mappings referenced in Theorem 3.1. First, we need the contraction mapping for implicit Euler, i.e.,

$$\mathbf{Q}_k(\mathbf{f}) = \mathbf{f}_k + \Delta t \mathbf{G}(\mathbf{f}), \quad (48)$$

where Δt satisfies (31). Next, we approximate \mathbf{Q}_k by the tensor

$$\tilde{\mathbf{Q}}_k(\mathbf{f}) = \mathfrak{T}_{\mathbf{r}_2}(\mathbf{f}_k + \Delta t \mathfrak{T}_{\mathbf{r}_1}(\mathbf{G}(\mathbf{f}))), \quad (49)$$

where \mathbf{r}_1 and \mathbf{r}_2 are multilinear ranks chosen to satisfying

$$\|\mathbf{A} - \mathfrak{T}_{\mathbf{r}_1}(\mathbf{A})\| \leq a\varepsilon/\Delta t, \quad (50)$$

$$\|\mathbf{B}_k - \mathfrak{T}_{\mathbf{r}_2}(\mathbf{B}_k)\| \leq b\varepsilon, \quad (51)$$

and

$$\mathbf{A} = \mathbf{G}(\mathbf{f}), \quad \mathbf{B}_k = \mathbf{f}_k + \Delta t \mathfrak{T}_{\mathbf{r}_1}(\mathbf{A}). \quad (52)$$

Clearly, if a and b are two positive constants satisfying $a + b = 1$ then we have

$$\left\| \mathbf{Q}_k(\mathbf{f}) - \tilde{\mathbf{Q}}_k(\mathbf{f}) \right\| \leq \varepsilon, \quad (53)$$

i.e., the tensor approximation (49) of the contraction mapping \mathbf{Q}_k satisfies the assumptions of Theorem 3.1. This allows us to write the implicit step-truncation Euler scheme as

$$\mathbf{y}^{[j+1]} = \mathbf{f}_k + \Delta t \mathbf{G} \left(\mathbf{f}_{k+1}^{[j]} \right), \quad (54)$$

$$\varepsilon_j = \frac{1 - \Delta t L_{\mathbf{G}}}{c} \left\| \mathbf{y}^{[j+1]} - \mathbf{f}_{k+1}^{[j]} \right\|, \quad (55)$$

$$\mathbf{f}_{k+1}^{[j+1]} = \mathfrak{T}_{r_2} \left[\mathbf{f}_k + \Delta t \mathfrak{T}_{r_1} \left(\mathbf{G} \left(\mathbf{f}_{k+1}^{[j]} \right) \right) \right]. \quad (56)$$

Note that in Equation (55) we set the Lipschitz constant $\hat{q} = \Delta t L_{\mathbf{G}}$ (see the discussion after Theorem 3.2).

4.1. Convergence analysis

The fixed point iterations defined in Theorem 3.1 are explicit. Hence, convergence of implicit step-truncation methods can be established in the setting of explicit step-truncation methods, i.e., by using techniques similar to those used in the proof of Theorem 2.1. Consistency of the implicit step-truncation Euler method (54)-(56) follows immediately from Corollary 3.2. In fact, denoting by $\mathbf{f}(t)$ the exact solution of the differential equation (4) we have

$$\left\| \mathbf{f}(\Delta t) - \mathbf{f}_1^{[j]} \right\| \leq \left\| \mathbf{f}(\Delta t) - \mathbf{f}_1 \right\| + \left\| \mathbf{f}_1 - \mathbf{f}_1^{[j]} \right\| \leq K_1 \Delta t^2 + G_c(\Delta t L_{\mathbf{G}}) \varepsilon_{\text{tol}}, \quad (57)$$

where K_1 is a local error constant, G_c is defined in (41), and ε_{tol} is the stopping tolerance. By selecting a positive constant B so that $\varepsilon_{\text{tol}} \leq B \Delta t^2$, we have that the method is consistent. Regarding stability of step-truncation implicit Euler, we can rely on the stability of the conventional implicit Euler method. To this end, suppose that $\hat{\mathbf{f}}_0$ and $\tilde{\mathbf{f}}_0$ are two initial conditions. We want to establish whether the implicit step-truncation Euler method is stable when we terminate the fixed point iterations after a consistent tolerance is met. This results in two different iteration counts, say j and m . By inspecting their difference, we see

$$\left\| \hat{\mathbf{f}}_1^{[j]} - \tilde{\mathbf{f}}_1^{[m]} \right\| \leq \left\| \hat{\mathbf{f}}_1^{[j]} - \hat{\mathbf{f}}_1 \right\| + \left\| \hat{\mathbf{f}}_1 - \tilde{\mathbf{f}}_1 \right\| + \left\| \tilde{\mathbf{f}}_1^{[m]} - \tilde{\mathbf{f}}_1 \right\|, \quad (58)$$

$$\leq (1 + 2L_{\mathbf{G}} \Delta t) \left\| \hat{\mathbf{f}}_0 - \tilde{\mathbf{f}}_0 \right\| + 2G_c(\Delta t L_{\mathbf{G}}) \varepsilon_{\text{tol}}. \quad (59)$$

Clearly, the method is stable, i.e., it satisfies (19), when $\varepsilon_{\text{tol}} \leq B \Delta t^2$. By applying Theorem 2.1, we conclude that the implicit step-truncation Euler method is convergent⁴.

⁴The condition $\varepsilon_{\text{tol}} \leq B \Delta t^2$ introduces a free parameter B . We shall see in section 5 that an analogous parameter appears in the implicit step-truncation midpoint method. There is a convenient value of B which we can use. Such value follows from the error term we find by applying the proposed fixed point iteration method, i.e., $E(\Delta t) = G_c(\Delta t L_{\mathbf{G}}) B \Delta t^2$. By setting $B = 1/G_c(0) = (1 - c)/(c + c^2)$, we see that the local error coefficient conveniently converges to 1 as $\Delta t \rightarrow 0$, thereby giving a negligible impact on error convergence rate.

5. Implicit step-truncation midpoint method

Consider the conventional implicit midpoint method⁵

$$\mathbf{f}_{k+1} = \mathbf{f}_k + \Delta t \mathbf{G} \left(\frac{\mathbf{f}_k + \mathbf{f}_{k+1}}{2} \right) \quad (60)$$

and the associated mapping

$$\mathbf{Q}_k(\mathbf{f}) = \mathbf{f}_k + \Delta t \mathbf{G} \left(\frac{\mathbf{f}_k + \mathbf{f}}{2} \right), \quad (61)$$

Clearly, \mathbf{Q}_k satisfies the Lipschitz continuity condition (assuming \mathbf{G} is Lipschitz)

$$\|\mathbf{Q}_k(\mathbf{f}) - \mathbf{Q}_k(\mathbf{g})\| \leq \frac{\Delta t L_{\mathbf{G}}}{2} \|\mathbf{f} - \mathbf{g}\| \quad \text{for all } \mathbf{f}, \mathbf{g} \in \mathcal{D}, \quad (62)$$

where $L_{\mathbf{G}}$ denotes the Lipschitz constant of \mathbf{G} . If $\Delta t < 2/L_{\mathbf{G}}$ then \mathbf{Q}_k is a (strict) contraction. It is worth noting that the upper bound $2/L_{\mathbf{G}}$ is twice the one we obtained for the implicit Euler method (see equation (30)). Hence, \mathbf{Q}_k in (61) allows for larger Δt relative to implicit Euler method, while also being a method of order 2, symmetric and symplectic.

To develop the implicit step-truncation midpoint method we follow the same steps as we did for the implicit step-truncation Euler. To this end, consider the following tensor approximation of the mapping \mathbf{Q}_k

$$\tilde{\mathbf{Q}}_k(\mathbf{f}) = \mathfrak{T}_{r_3} \left(\mathbf{f}_k + \Delta t \mathfrak{T}_{r_2} \left[\mathbf{G} \left(\frac{1}{2} \mathfrak{T}_{r_1}(\mathbf{f}_k + \mathbf{f}) \right) \right] \right), \quad (63)$$

The multilinear ranks r_i are chosen to satisfy

$$\|\mathbf{A}_k - \mathfrak{T}_{r_1}(\mathbf{A}_k)\| \leq \frac{2a\varepsilon}{\Delta t L_{\mathbf{G}}}, \quad (64)$$

$$\|\mathbf{B}_k - \mathfrak{T}_{r_2}(\mathbf{B}_k)\| \leq \frac{b\varepsilon}{\Delta t}, \quad (65)$$

$$\|\mathbf{C}_k - \mathfrak{T}_{r_3}(\mathbf{C}_k)\| \leq c\varepsilon, \quad (66)$$

where

$$\mathbf{A}_k = \mathbf{f}_k + \mathbf{f}, \quad \mathbf{B}_k = \mathbf{G} \left[\mathfrak{T}_{r_1} \left(\frac{\mathbf{A}_k}{2} \right) \right], \quad \mathbf{C}_k = \mathbf{f}_k + \Delta t \mathfrak{T}_{r_2}(\mathbf{B}_k). \quad (67)$$

As before, if a , b and c are three positive constants satisfying $a + b + c = 1$ then it is straightforward to show (through the use of two triangle inequalities and an appeal to Lipschitz continuity) that

$$\|\mathbf{Q}_k(\mathbf{f}) - \tilde{\mathbf{Q}}_k(\mathbf{f})\| \leq \varepsilon. \quad (68)$$

In other words, the tensor approximation (63) of the contraction mapping (61) satisfies the assumptions of Theorem 3.1. This allows us to write the implicit step-truncation midpoint method

⁵As is well known, the implicit midpoint method 60 is a symplectic symmetric integrator of order 2 (see, e.g., [23]).

as

$$\mathbf{g}^{[j+1]} = \mathbf{f}_k + \Delta t \mathbf{G} \left(\frac{1}{2} \left(\mathbf{f}_k + \mathbf{f}_{k+1}^{[j]} \right) \right), \quad (69)$$

$$\varepsilon_j = \frac{2 - \Delta t L_{\mathbf{G}}}{2c} \left\| \mathbf{g}^{[j+1]} - \mathbf{f}_{k+1}^{[j]} \right\|, \quad (70)$$

$$\mathbf{f}_{k+1}^{[j+1]} = \mathfrak{T}_{r_3} \left(\mathbf{f}_k + \Delta t \mathfrak{T}_{r_2} \left[\mathbf{G} \left(\frac{1}{2} \mathfrak{T}_{r_1} \left(\mathbf{f}_k + \mathbf{f}_{k+1}^{[j]} \right) \right) \right] \right). \quad (71)$$

5.1. Convergence analysis

Convergence of the step-truncation implicit midpoint method can be established by following the arguments of equations (57), (58), and (59). Consistency gives

$$\left\| \mathbf{f}(\Delta t) - \mathbf{f}_1^{[j]} \right\| \leq K_1 \Delta t^3 + G_c (\Delta t L_{\mathbf{G}} / 2) \varepsilon_{\text{tol}}, \quad (72)$$

where K_1 is a local error coefficient of the implicit midpoint method. Stability follows by applying inequality (58) to the implicit midpoint method. This gives

$$\left\| \hat{\mathbf{f}}_1^{[j]} - \tilde{\mathbf{f}}_1^{[m]} \right\| \leq (1 + L_{\mathbf{G}} \Delta t) \left\| \hat{\mathbf{f}}_0 - \tilde{\mathbf{f}}_0 \right\| + 2G_c (\Delta t L_{\mathbf{G}} / 2) \varepsilon_{\text{tol}}. \quad (73)$$

Therefore, in the limit of $\Delta t \rightarrow 0$, we see that there exists a constant $B > 0$ so that $\varepsilon_{\text{tol}} \leq B \Delta t^3$. Just as with the implicit Euler method, we may select $B = 1/G_c(0) = (1 - c)/(c + c^2)$.

6. Absolute stability analysis

The notion of absolute stability is related to the condition (19), but is not concerned with the limit $\Delta t \rightarrow 0$. Instead, we ask what the largest allowable Δt is before a step-truncation method fails to produce a solution that decays to zero when applied to the linear test problem

$$\frac{d\mathbf{y}}{dt} = \lambda \mathbf{y}, \quad \text{Re}(\lambda) < 0. \quad (74)$$

By discretizing (74) using an implicit or explicit step-truncation method we obtain the linear update

$$\mathbf{y}_{k+1} = S(\Delta t \lambda) \mathbf{y}_k \quad (75)$$

In Figure 3 we plot the values of $z = \Delta t \lambda$ so that the discrete time update operator S has amplitude equal to one, i.e., $|S(z)| = 1$. In the case of explicit step-truncation methods, the guaranteed stability region is the same as the corresponding conventional scheme without truncation [38, 37]. Since our implicit methods are essentially modifications of known methods, we also have a direct relationship. Since we only require that $\mathbf{Q}_k(\mathbf{f})$ is a contraction, we can simply intersect the disc of complex numbers where this holds with the underlying method's stability region. This is the same stability condition as an implicit method with a standard fixed point iteration [24]. The aforementioned intersection can cause sharp corners in the stability region, as seen in Figure 3.

The result is that the implicit midpoint stability region is similar to that of the explicit midpoint method, but also contains the imaginary axis. This allows for enhanced stability for problems with imaginary eigenvalues such as the Schrödinger equation problem discussed hereafter. In special cases of fixed-rank step-truncation methods, the stability region of the implicit methods can be expanded to cover the entire left half complex plane by using a splitting method.

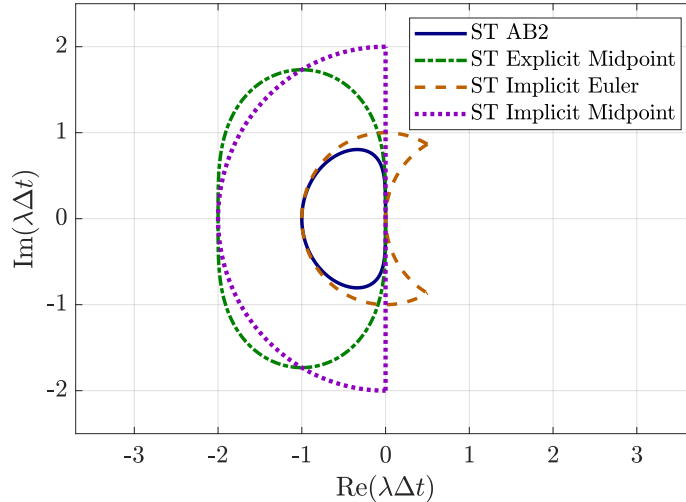


Figure 3: Boundary of the regions of absolute stability for various step-truncation (ST) methods. The methods are absolutely stable inside the regions.

7. Numerical results

In this section we investigate the performance of the proposed implicit step-truncation methods in three numerical applications involving time-dependent PDEs. Specifically, we study the Allen-Cahn equation [32] in two spatial dimensions, a Fokker-Planck equation [36] in four dimensions, and the nonlinear Schrödinger equation [41] in six dimensions.

7.1. Allen-Cahn equation

The Allen-Cahn equation is a reaction-diffusion equation that describes the process of phase separation in multi-component alloy systems [1, 2]. In its simplest form, the equation includes a low-order polynomial non-linearity (reaction term) and a diffusion term, which leads to the stiff PDE [27]

$$\frac{\partial f}{\partial t} = \varepsilon \Delta f + f - f^3. \quad (76)$$

In our application, we set $\varepsilon = 0.1$, and solve (76) on a two-dimensional flat torus. The initial condition is set as

$$f_0(x, y) = u(x, y) - u(x, 2y) + u(3x + \pi, 3y + \pi) - 2u(4x, 4y) + 2u(5x, 5y), \quad (77)$$

where

$$u(x, y) = \frac{\left[e^{-\tan^2(x)} + e^{-\tan^2(y)} \right] \sin(x) \sin(y)}{1 + e^{|\csc(-x/2)|} + e^{|\csc(-y/2)|}}. \quad (78)$$

We discretize (76) in space using the two-dimensional Fourier pseudospectral collocation method [25] with 256×256 points in $\Omega = [0, 2\pi]^2$. This results in a matrix ODE in the form of (4). We

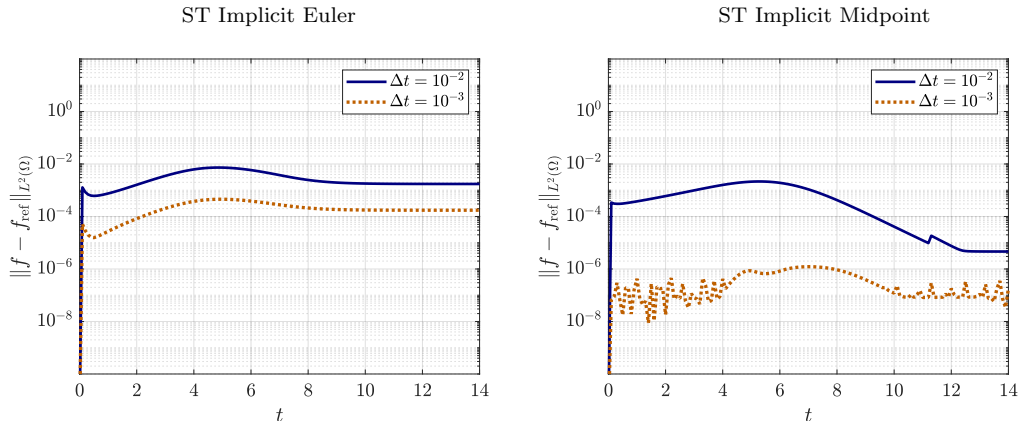


Figure 4: Error versus time for step-truncation numerical solutions of Allen-Cahn equation (81) in dimension $d = 2$ with initial condition (77).

truncate the initial condition to absolute and relative SVD tolerances of 10^{-9} , which yields an initial condition represented by a 256×256 matrix of rank 90. We also solve the problem with a benchmark variable step size RK4 method with absolute tolerance 10^{-14} , which we refer to as f_{ref} . In Figure 4 we compare the performance the proposed step truncation (ST) implicit methods, i.e., Euler backward (order 1) and midpoint (order 2) methods. The solver was run with stopping tolerance of Algorithm 1 set to 2.2×10^{-8} and time integration was halted at $t = 14$, i.e., when the steady state condition $\|\partial f / \partial t\| \leq 2 \times 10^{-3}$ is satisfied. After this point, the errors stay bounded near the final values plotted above, until eventually $\|\partial f / \partial t\| \leq 10^{-7}$ at $t = 25$. In Figure 5, we plot the solution rank versus time. Due to the smoothing properties of the Laplacian, the high frequencies in the initial condition are quickly damped out (stiffness). This allows the numerical tensor method of produce an excellent low-rank estimate of the solution. Due to the rapidly decaying rank for this problem, we have plotted the rank it in log scale. In Figure 6, we compare the performance of proposed implicit step truncation midpoint method to the second-order step-truncation explicit midpoint method (see [37])

$$\mathbf{f}_{k+1} = \mathfrak{T}_{\mathbf{r}_3} \left(\mathbf{f}_k + \Delta t \mathfrak{T}_{\mathbf{r}_2} \left[\mathbf{G} \left(\mathbf{f}_k + \frac{\Delta t}{2} \mathfrak{T}_{\mathbf{r}_1} (\mathbf{G}(\mathbf{f}_k)) \right) \right] \right), \quad (79)$$

where the ranks $\mathbf{r}_1, \mathbf{r}_2, \mathbf{r}_3$ are time-dependent and found with the truncation tolerances

$$\varepsilon_{\mathbf{r}_3} \leq A \Delta t^3, \quad \varepsilon_{\mathbf{r}_2} \leq B \Delta t^2, \quad \varepsilon_{\mathbf{r}_1} \leq G \Delta t. \quad (80)$$

It is seen that the explicit step-truncation midpoint method is “less stable” than the implicit one, blowing up when $\Delta t = 10^{-3}$. Moreover, in the rank-adaptive setting we consider here the time step Δt is tied to rank through the tensor truncation tolerances in equation (80). This implies that as $\Delta t \rightarrow 0$, we must retain more and more singular values, maxing out the rank and thereby giving up all gains from low-rank compression. On the other hand, if Δt gives an unstable iteration, then one can reasonably expect the singular values to increase, hence increasing the rank. We see both these problems with the step-truncation explicit midpoint method, giving only a narrow region of

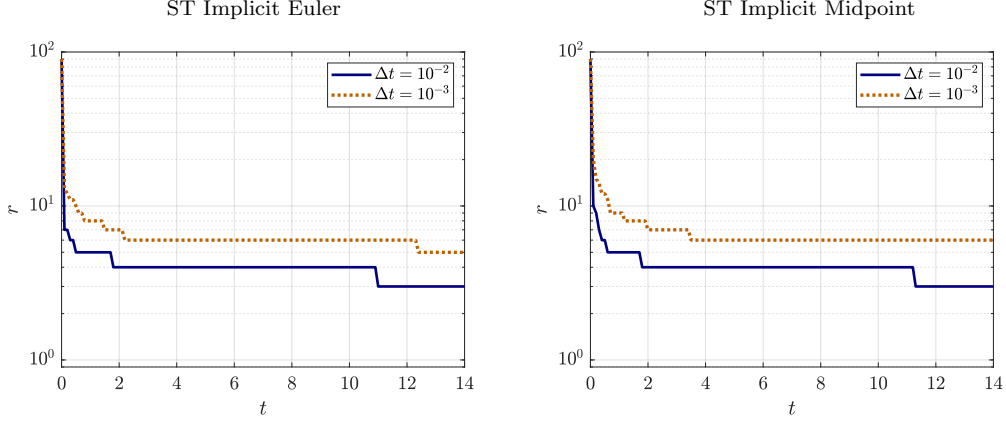


Figure 5: Rank versus time for step-truncation numerical solutions of Allen-Cahn equation (81) in dimension $d = 2$ with initial condition (77).

acceptable time step sizes (see Figure 6). By expanding the stability region by the use of implicit methods, we also expand this range of acceptable step sizes for the same accuracy.

7.2. Fokker-Planck equation

Consider the Fokker-Planck equation

$$\frac{\partial f(\mathbf{x}, t)}{\partial t} = - \sum_{i=1}^d \frac{\partial}{\partial x_i} (\mu_i(\mathbf{x}) f(\mathbf{x}, t)) + \frac{\sigma^2}{2} \sum_{i=1}^d \frac{\partial^2 f(\mathbf{x}, t)}{\partial x_i^2} \quad (81)$$

on a four-dimensional ($d = 4$) flat torus $\Omega = [0, 2\pi]^4$. The components of the drift term are chosen as

$$\mu_i(\mathbf{x}) = (\gamma(x_{i+1}) - \gamma(x_{i-2}))\xi(x_{i-1}) - \phi(x_i), \quad i = 1, \dots, d, \quad (82)$$

where $\gamma(x) = \sin(x)$, $\xi(x) = \exp(\sin(x)) + 1$, and $\phi(x) = \cos(x)$ are 2π -periodic functions. In (82) we set $x_{i+d} = x_i$. For this particular drift field, the right side of (81) can be split into a component tangential to the tensor manifold \mathcal{H}_r and a component that is non-tangential as

$$\frac{\partial f(\mathbf{x}, t)}{\partial t} = \underbrace{\sum_{i=1}^d \left(-\gamma(x_{i+1})\xi(x_{i-1}) \frac{\partial f(\mathbf{x}, t)}{\partial x_i} + \gamma(x_{i-2})\xi(x_{i-1}) \frac{\partial f(\mathbf{x}, t)}{\partial x_i} \right)}_{\text{Not tangential}} + \underbrace{\left(\frac{\partial}{\partial x_i} \phi(x_i) f(\mathbf{x}, t) + \frac{\sigma^2}{2} \frac{\partial^2 f(\mathbf{x}, t)}{\partial x_i^2} \right)}_{\text{tangential}}. \quad (83)$$

We solve (83) using an operator splitting method. To this end, we notice that there are $3d$ many terms in the summation above, and therefore we first solve d many time dependent PDEs which

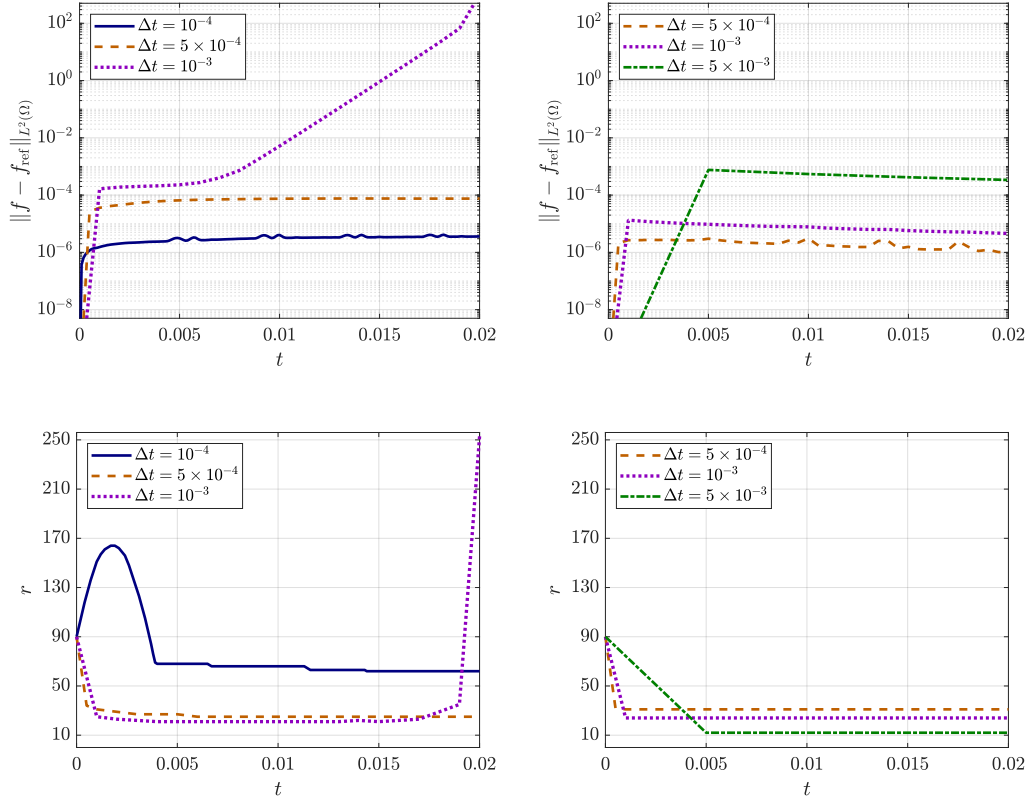


Figure 6: Comparison between $L^2(\Omega)$ errors and tensor rank r of step-truncation explicit and implicit midpoint integrators applied to the Allen-Cahn equation (76). It is seen that the implicit step-truncation midpoint integrator can handle non-linearity, stiffness and rank increase in an effective way, while retaining the same level of accuracy of the explicit step-truncation midpoint method.

are tangent to the tensor manifold,

$$\frac{\partial g_i}{\partial t} = \frac{\partial}{\partial x_i} \phi(x_i) g_i + \frac{\sigma^2}{2} \frac{\partial^2 g_i}{\partial x_i^2}, \quad i = 1, \dots, d. \quad (84)$$

Then we solve the non-tangential equations in two batches,

$$\frac{\partial u_j}{\partial t} = \gamma(x_{i+1}) \xi(x_{i-1}) \frac{\partial u_j}{\partial x_i}, \quad j = 1, \dots, d \quad (85)$$

$$\frac{\partial u_k}{\partial t} = \gamma(x_{i-2}) \xi(x_{i-1}) \frac{\partial u_k}{\partial x_i}, \quad k = 2, \dots, 2d. \quad (86)$$

This yields the order 1 (Lie-Trotter) approximation $f(\mathbf{x}, \Delta t) = u_{2d}(\mathbf{x}, \Delta t) + O(\Delta t^2)$. We also use these same list of PDEs for the order 2 (Strang) splitting integrator. We chose the initial condition

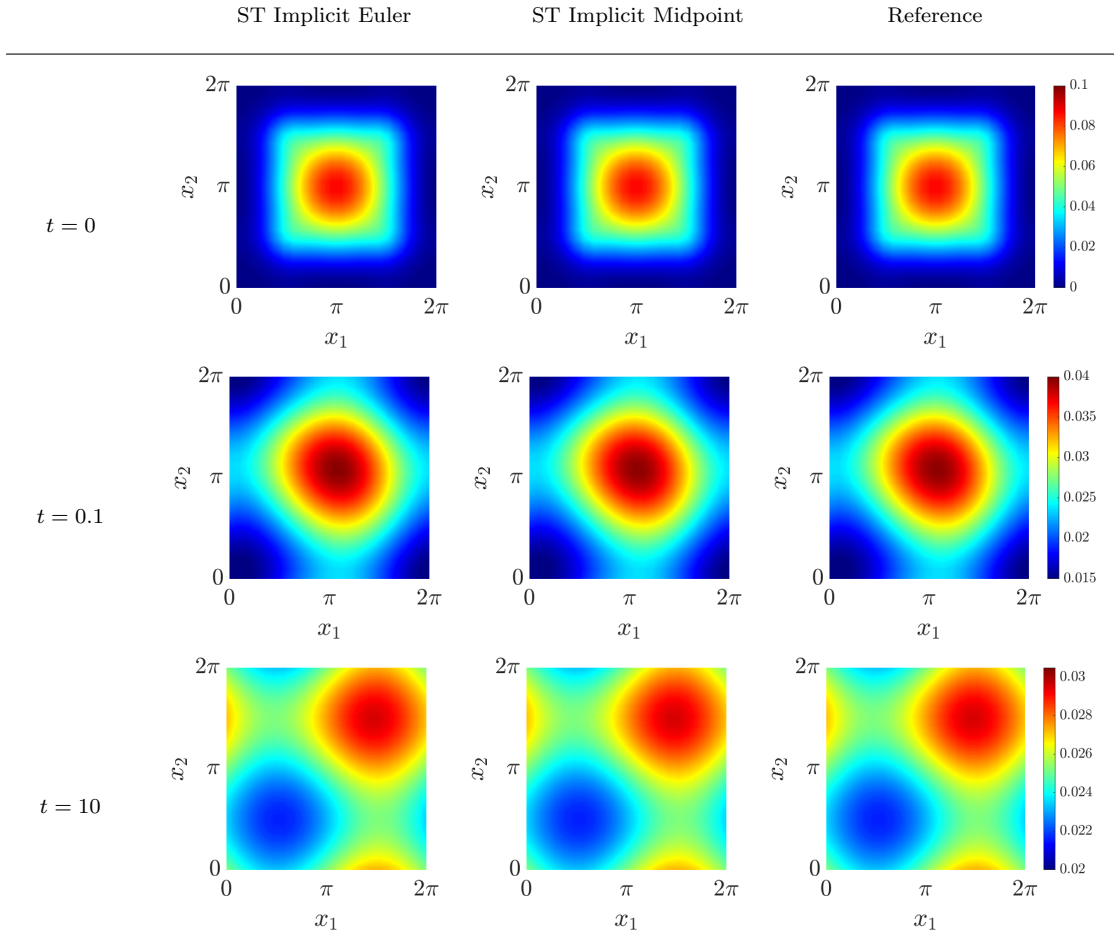


Figure 7: Marginal probability density function (88) obtained by integrating numerically the Fokker–Planck equation (81) in dimension $d = 4$ with $\sigma = 5$ and initial condition (87) with two rank-adaptive methods, namely the step-truncation implicit Euler (section 4) and the step-truncation implicit midpoint method (section 5). The reference solution is obtained using a variable time step RK4 method with absolute tolerance of 10^{-14} . These solutions are computed on a grid with $20 \times 20 \times 20 \times 20$ interior points (evenly spaced). The steady state is determined for this computation by halting execution when $\|\partial f_{\text{ref}}/\partial t\|_2$ is below a numerical threshold of 10^{-8} . This happens at approximately $t \approx 10$ for the initial condition (87).

as

$$f_0(x_1, x_2, x_3, x_4) = \frac{1}{m_0} \sum_{j=1}^M \left(\prod_{i=1}^4 \frac{\sin((2j-1)x_i - \pi/2) + 1}{2^{2(j-1)}} + \prod_{i=1}^4 \frac{\exp(\cos(2jx_i + \pi))}{2^{2j-1}} \right), \quad (87)$$

where m_0 is a normalization constant. This gives an HTucker tensor with rank bounded by $2M$. We set $M = 10$ to give ranks bounded by 20. We discretize (81)-(87) in Ω with the Fourier pseudospectral collocation method on a tensor product grid with $N = 21$ evenly-spaced points along each coordinate x_i , giving the total number of points $N^4 = 194481$. This number corresponds

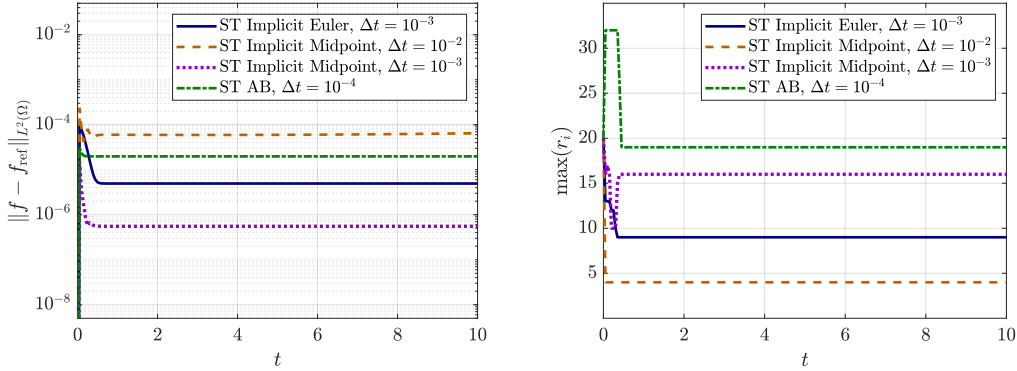


Figure 8: $L^2(\Omega)$ error and rank versus time for numerical solutions of Fokker–Planck equation (81) in dimension $d = 4$ with initial condition (87). The rank plotted here is the largest rank for all tensors being used to represent the solution in HT format. Rank of the reference solution is in HT format.

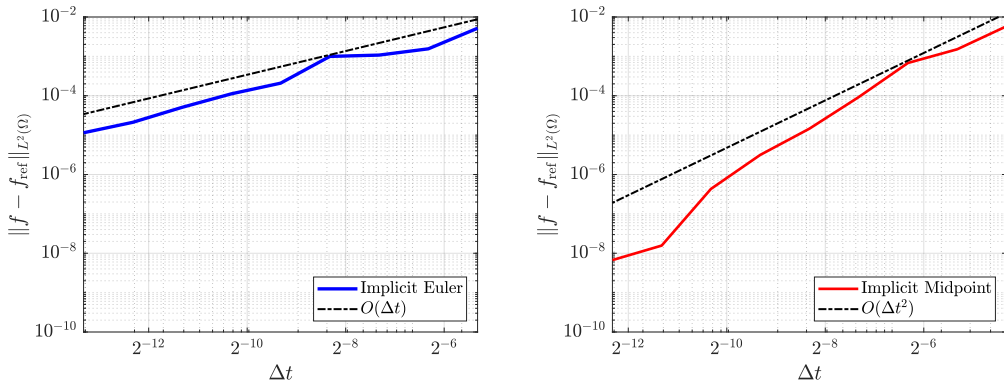


Figure 9: Global $L^2(\Omega)$ errors for different rank-adaptive step-truncation implicit methods found by solving equation (81) up to time $T = 0.1$ with $\sigma = 2$. The reference solution is a variable time step RK4 method with absolute tolerance of 10^{-14} .

to the number of entries in the tensor $\mathbf{f}(t)$ appearing in equation (4). Also, we set $\sigma = 5$ in (81) so that the PDE is sufficiently stiff. In Figure 7 we compare the time snapshots of the marginal probability density function (PDF)

$$f_{12}(x_1, x_2) = \int_0^{2\pi} \int_0^{2\pi} f(x_1, x_2, x_3, x_4) dx_3 dx_4 \tag{88}$$

we obtained with implicit step-truncation Euler and midpoint methods, as well as the reference marginal PDF. The solution very quickly relaxes to become nearly uniform by $t = 0.1$ (stiffness), then slowly rises to its steady state distribution by $t = 10$. In Figure 8 we study accuracy and rank

of the proposed implicit step-truncation methods in comparison with the rank-adaptive explicit Adams-Bashforth (AB) method of order 2 (see [37]). It is seen that the step-truncation implicit midpoint method with time step $\Delta t = 10^{-3}$ achieves higher accuracy and smaller rank than the step-truncation explicit Adams-Bashforth method with $\Delta t = 10^{-4}$. Moreover, the step-truncation implicit midpoint method can stably integrate the Fokker-Planck equation (81) with $\Delta t = 10^{-2}$, while retaining reasonable accuracy and achieving very low rank. On the other hand, the step-truncation explicit AB2 method requires time step near 10^{-4} for stability. This causes a penalty in the rank, since as the time step is made small, the rank must be large to maintain convergence order [37]. The step-truncation implicit midpoint method seems to be the best among the three methods, with error of approximately 10^{-6} and rank lower than the step-truncation explicit AB2 method at steady state. Overall, implicit step-truncation methods perform extremely well on linear problems of this form, especially when the right hand side is explicitly written as a sum of tensor products of one-dimensional operators. Finally, in Figure 9 we plot the convergence rate of the step-truncation implicit Euler and implicit midpoint methods. As expected, the convergence rates are of order 1 and order 2 respectively, verifying Theorem 2.1.

7.3. Nonlinear Schrödinger equation

The nonlinear Schrödinger equation is complex-valued PDE of classical physics whose principal applications are wave propagation in nonlinear optical fibers, and Bose-Einstein condensates [41, 39]. The equation can be written as⁶

$$\frac{\partial \phi(\mathbf{x}, t)}{\partial t} = \frac{i}{2} \Delta \phi(\mathbf{x}, t) - iV(\mathbf{x})\phi(\mathbf{x}, t) - i\varepsilon |\phi(\mathbf{x}, t)|^2 \phi(\mathbf{x}, t). \quad (90)$$

where $V(\mathbf{x})$ is the particle interaction potential. In our example, we consider 6 particles trapped on a line segment in the presence of a double well potential defined as

$$V(\mathbf{x}) = \sum_{k=1}^6 W(x_k), \quad W(x_k) = \left[1 + e^{\cos(x_k)^2} + \frac{3}{4} \left(1 + e^{\sin(x_k)^2} \right) \right] \eta_\theta(x_k). \quad (91)$$

Here, $W(x_k)$ is a potential with barriers at $x_k = 0$ and $x_k = \pi$ (see Figure 10). The function $\eta_\theta(x_i)$ is a mollifier which converges weakly to $1 + \delta(x_i) + \delta(x_i - \pi)$ as $\theta \rightarrow 0$. One such mollifier is

$$\eta_\theta(x) = 1 + \frac{1}{\sqrt{2\pi\theta}} \left(\exp \left[-\frac{x^2}{2\theta^2} \right] + \exp \left[-\frac{(x - \pi)^2}{2\theta^2} \right] \right). \quad (92)$$

As $\theta \rightarrow 0$, the weak limit of η_θ translates to zero Dirichlet boundary conditions on the domain $\Omega = [0, \pi]^6$. The Dirichlet conditions naturally allow us to use a discrete sine transform to compute the Laplacian's differentiation matrices. We discretize the domain Ω on a uniform grid with 35 points per dimension. This gives us a tensor with $35^6 = 838265625$ entries, or 14.7 Gigabytes per

⁶As is well-known, the nonlinear Schrödinger equation (90) is a Hamiltonian PDE which can be derived as a stationary point of the energy density (Hamilton's functional)

$$H(\phi) = \int_{\Omega} \frac{1}{4} \|\nabla \phi\|^2 + \frac{1}{2} V(\mathbf{x}) |\phi(\mathbf{x}, t)|^2 + \frac{\varepsilon}{4} |\phi|^4 \, d\mathbf{x}. \quad (89)$$

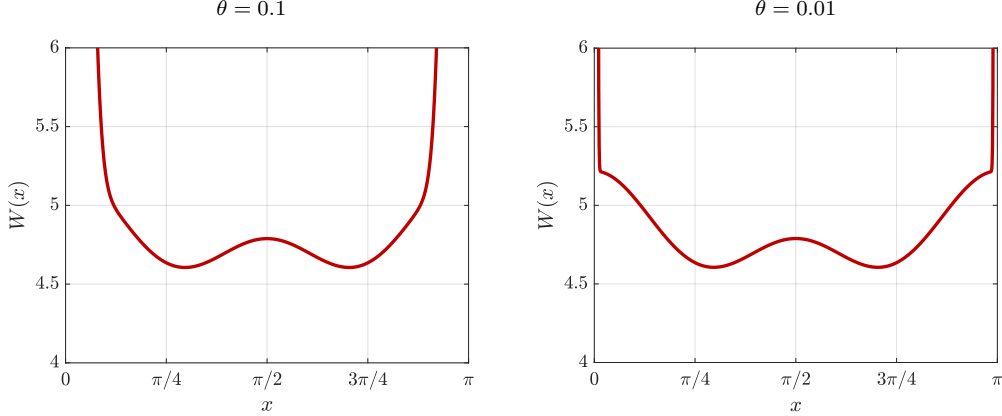


Figure 10: Double well potential (91)-(92) for different values of θ . It is seen that as $\theta \rightarrow 0$, the potential barrier at $x = 0$ and $x = \pi$ becomes infinitely high. This is identical to the well-known homogeneous boundary conditions for particles trapped in a box.

temporal solution snapshot if we store the tensor in a double precision IEEE 754 floating point format. We choose a product of pure states for our initial condition, i.e.,

$$\phi(\mathbf{x}, 0) = \prod_{k=1}^6 \frac{6^{1/6} 4k}{2k\pi - \sin(2\pi k)} \sin(kx_k), \quad (93)$$

The normalizing constant $6^{1/6} 4k / (2k\pi - \sin(2\pi k))$ guarantees that the wavefunction has an initial mass of 6 particles. We now apply an operator splitting method to solve (90). The linear components are all tangential to the tensor manifold \mathcal{H}_r , and have a physical interpretation. Specifically,

$$\frac{\partial g_k}{\partial t} = \frac{i}{2} \frac{\partial^2 g_k}{\partial x_k^2} - iW(x_k)g_k, \quad k = 1, \dots, 6, \quad (94)$$

is a sequence of one-dimensional linear Schrödinger equations. The non-tangential part reduces to

$$\frac{du}{dt} = i\varepsilon|u|^2u, \quad (95)$$

which may be interpreted as an ODE describing all pointwise interactions of the particles. Here we set $\varepsilon = 10^{-4}$ to model weak interactions. Clearly, the linear terms in (90) have purely imaginary eigenvalues. Therefore to integrate the semi-discrete form of (90) in time we need a numerical scheme that has the imaginary axis within its stability region. As seen from Figure 3, the proposed implicit step-truncation methods are the most suitable for this purpose. Since implicit step-truncation Euler method introduces a significant damping, thereby exacerbating inaccuracy due to discrete time stepping, we apply the implicit step-truncation midpoint method. We set $\Delta t = 5 \times 10^{-2}$ and a truncation tolerance in Algorithm 1 of $10^2 \Delta t^3$. In Figure 11 we plot the time-dependent marginal probability density functions for the joint position variables (x_k, x_{k+1}) , $k = 1, 3, 5$. Such probability densities are defined as

$$p(x_1, x_2, t) = \frac{1}{6} \int_{[0,1]^4} \phi^*(\mathbf{x}, t) \phi(\mathbf{x}, t) dx_3 dx_4 dx_5 dx_6, \quad (96)$$

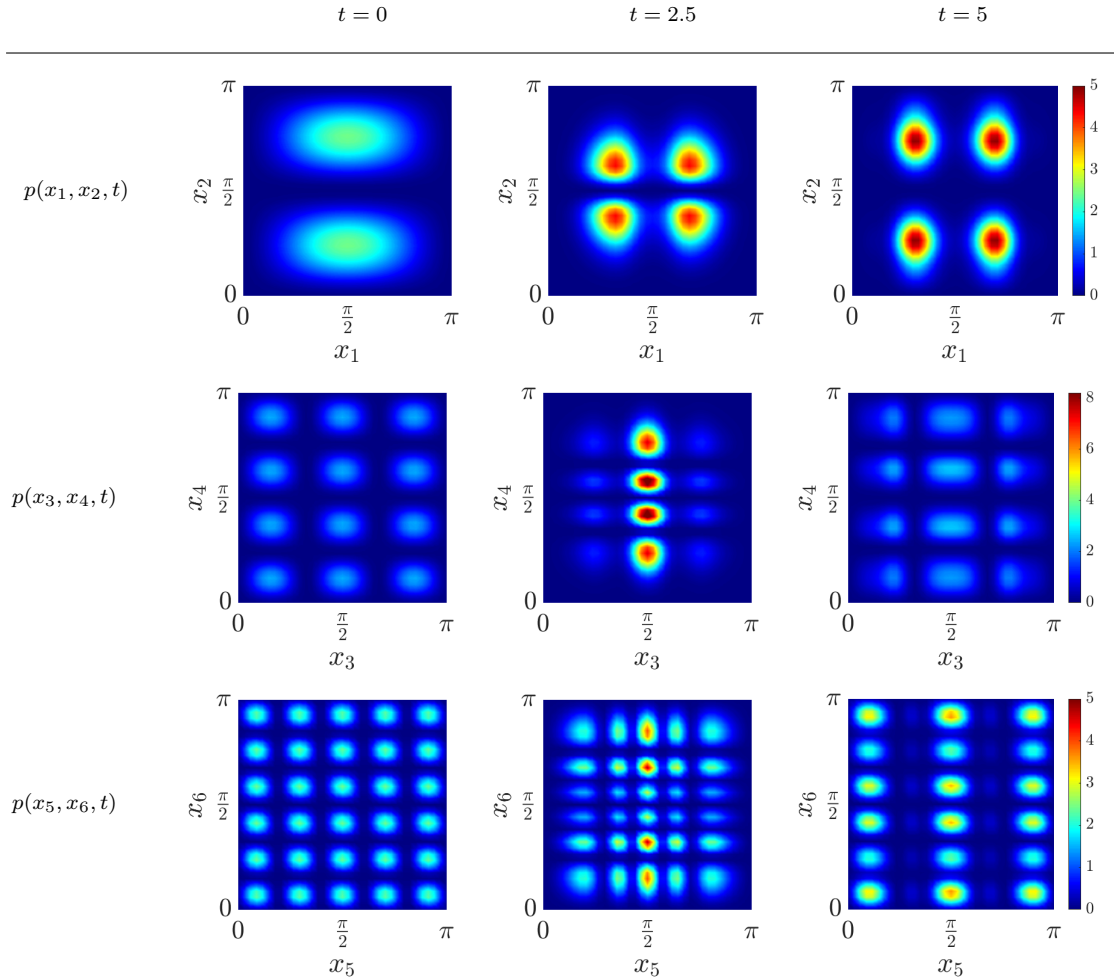


Figure 11: Marginal probability density functions representing particle positions generated by the nonlinear Schrödinger equation (90) with $\varepsilon = 10^{-4}$, interaction potential (91) and initial condition (93).

and analogously for $p(x_3, x_4, t)$ and $p(x_5, x_6, t)$. It is seen that the lower energy pure states (position variables (x_1, x_2)) quickly get trapped in the two wells, oscillating at their bottoms. Interestingly, at $t = 2.5$ it appears that particle x_3 is most likely to be observed in between the two wells whenever the particle x_4 is in a well bottom.

In Figure 12(a), we plot the rank over time for this problem. The rank also has physical meaning. A higher rank HT tensor is equivalent to a wavefunction with many entangled states, regardless of which $L^2(\Omega)$ basis we choose. In the example discussed in this section, the particles interacting over time monotonically increase the rank. We emphasize that the nonlinearity in (90) poses a significant challenge to tensor methods. In fact, in a single application of the function $i\varepsilon|u|^2u$, we may end up tripling the rank. This can be mitigated somewhat by using the approximate element-wise tensor multiplication routine. Even so, if Algorithm 1 requires many dozens of iterations to

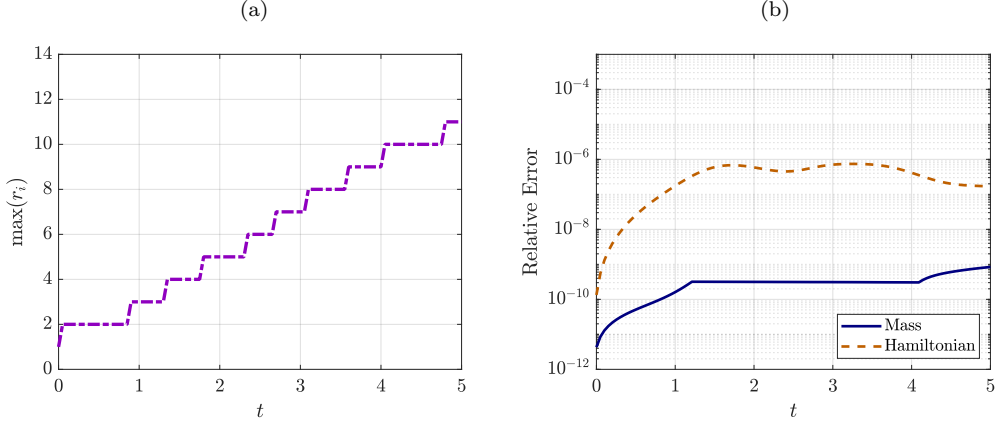


Figure 12: (a) Maximum tensor rank versus time, and (b) relative error in the the solution mass and Hamiltonian (89) for nonlinear Schrödinger equation (90) in dimension $d = 6$, with $\varepsilon = 10^{-4}$, interaction potential (91) and initial condition (93).

halt, the rank may grow very rapidly in a single time step, causing a slowing due to large array storage. This problem is particularly apparent when $\varepsilon \approx 1$ or if Δt is made significantly smaller, e.g. $\Delta t = 10^{-4}$. A more effective way of evaluating nonlinear functions on tensors decompositions would certainly mitigate this issue. In Figure 12(b), we plot the relative error of the solution mass and the Hamiltonian (89) over time. The relative errors hover around 10^{-10} and 10^{-6} , respectively. It is remarkable that even though the additional tensor truncation done after the inner loop of the implicit solver in principle destroys the symplectic properties of the midpoint method, the mass and Hamiltonian are still preserved with high accuracy.

Acknowledgements

This research was supported by the U.S. Air Force Office of Scientific Research grant FA9550-20-1-0174, and by the U.S. Army Research Office grant W911NF1810309.

Appendix A. Proof of Theorem 3.1

To prove Theorem 3.1 we first estimate the distance $\|\mathbf{y}^{[j+1]} - \mathbf{f}^{[j]}\|$ using induction. Then we bound $\|\mathbf{f}^{[j+1]} - \mathbf{f}^{[j]}\|$ in terms of $\|\mathbf{y}^{[j+1]} - \mathbf{f}^{[j]}\|$. This fact is used to show that the $\mathbf{f}^{[j]}$ form a Cauchy sequence. Finally we show that $\varepsilon_j \rightarrow 0$ as $j \rightarrow \infty$, which implies the sequence $\mathbf{f}^{[j]}$ tends to a fixed point of \mathbf{Q}_k .

Proof. Consider first time step, i.e., $j = 1$. It is straightforward to show that $\|\mathbf{y}^{[2]} - \mathbf{f}^{[1]}\|$ is bounded by a polynomial in q multiplied by the norm $\|\mathbf{y}^{[1]} - \mathbf{f}^{[0]}\|$. In fact, by using equations (36)-(38) and the triangle inequality we obtain

$$\begin{aligned} \|\mathbf{y}^{[2]} - \mathbf{f}^{[1]}\| &\leq q \left(\|\mathbf{f}^{[1]} - \mathbf{y}^{[1]}\| + \|\mathbf{y}^{[1]} - \mathbf{f}^{[0]}\| \right) + \|\mathbf{y}^{[1]} - \mathbf{f}^{[1]}\| \\ &\leq (c(1-q) + q) \|\mathbf{y}^{[1]} - \mathbf{f}^{[0]}\|. \end{aligned}$$

Now define $g_c(q) = c(1 - q) + q$. Clearly, $g_c(0) = c$ and $g_c(1) = 1$. Moreover, $g_c(q)$ is monotonically increasing since $g'_c(q) = 1 - c > 0$. Assume that $\|\mathbf{y}^{[j]} - \mathbf{f}^{[j-1]}\| \leq (g_c(q))^{j-1} \|\mathbf{y}^{[1]} - \mathbf{f}^{[0]}\|$. By following similar steps as above, we see that replacing $\mathbf{f}^{[j]}$ with $\mathbf{y}^{[j]}$ yields error ε_{j-1} . Therefore, we have the induction

$$\begin{aligned} \|\mathbf{y}^{[j+1]} - \mathbf{f}^{[j]}\| &\leq \|\mathbf{y}^{[j+1]} - \mathbf{y}^{[j]}\| + \varepsilon_{j-1} \\ &\leq q \|\mathbf{y}^{[j]} - \mathbf{f}^{[j-1]}\| + (1 + q)\varepsilon_{j-1} \\ &\leq g_c(q) \|\mathbf{y}^{[j]} - \mathbf{f}^{[j-1]}\| \\ &\leq (g_c(q))^j \|\mathbf{y}^{[1]} - \mathbf{f}^{[0]}\|. \end{aligned} \tag{A.1}$$

At this point we can use the estimate (A.1) to find $\|\mathbf{f}^{[j+1]} - \mathbf{f}^{[j]}\|$. To this end, we apply a similar technique as above we find a coefficient multiplying $\|\mathbf{y}^{[j+1]} - \mathbf{f}^{[j]}\|$ which depends on q . Specifically,

$$\begin{aligned} \|\mathbf{f}^{[j+1]} - \mathbf{f}^{[j]}\| &\leq \|\mathbf{f}^{[j+1]} - \mathbf{y}^{[j+1]}\| + \|\mathbf{y}^{[j+1]} - \mathbf{f}^{[j]}\| \\ &\leq \varepsilon_j + \|\mathbf{y}^{[j+1]} - \mathbf{f}^{[j]}\| = \left(c \frac{1-q}{1+q} + 1\right) \|\mathbf{y}^{[j+1]} - \mathbf{f}^{[j]}\|. \end{aligned} \tag{A.2}$$

By using (A.1) we obtain

$$\|\mathbf{f}^{[j+1]} - \mathbf{f}^{[j]}\| \leq \left(c \frac{1-q}{1+q} + 1\right) (g_c(q))^j \|\mathbf{y}^{[1]} - \mathbf{f}^{[0]}\|. \tag{A.3}$$

We will now use this estimate to show that $\mathbf{f}^{[j]}$ is a Cauchy sequence. To this end, let $m, n \in \mathbb{N}$ with $m > n$. Then the iterates satisfy

$$\begin{aligned} \|\mathbf{f}^{[m]} - \mathbf{f}^{[n]}\| &\leq \sum_{j=n}^{m-1} \|\mathbf{f}^{[j+1]} - \mathbf{f}^{[j]}\| \\ &\leq g_c(q)^n \left(c \frac{1-q}{1+q} + 1\right) \|\mathbf{y}^{[1]} - \mathbf{f}^{[0]}\| \sum_{j=0}^{m-n-1} (g_c(q))^j \\ &\leq \frac{g_c(q)^n}{1 - g_c(q)} \left(c \frac{1-q}{1+q} + 1\right) \|\mathbf{y}^{[1]} - \mathbf{f}^{[0]}\|. \end{aligned}$$

Since $0 \leq g_c(q) < 1$ we have that the iterates are Cauchy. Moreover \mathcal{D} is closed, and therefore the sequence $\mathbf{f}^{[j]}$ converges. Finally, noting that $\varepsilon_j \rightarrow 0$ for $j \rightarrow \infty$ and recalling (37) we conclude that

$$\lim_{j \rightarrow \infty} \|\mathbf{Q}_k(\mathbf{f}^{[j]}) - \mathbf{f}^{[j]}\| = \frac{1+q}{c(1-q)} \lim_{j \rightarrow \infty} \varepsilon_j = 0,$$

i.e., the limit point of the sequence $\mathbf{f}^{[j]}$ is a fixed point of \mathbf{Q}_k . Moreover, it is the only fixed point, as \mathbf{Q}_k is a contraction.

□

Appendix B. Step-truncation Adams-Moulton methods

In this Appendix we show how to derive implicit step-truncation schemes corresponding to arbitrary implicit multistep methods. First, we note that the above discussion for equations (24) and (30) implies the following lemma.

Lemma B1 (sufficient condition for contraction mapping) *Let \mathbf{W} be a locally Lipschitz map with constant $L_{\mathbf{W}}$. Let $\gamma > 0$ satisfy $\gamma L_{\mathbf{W}} < 1$. Then for any fixed $\mathbf{y} \in \mathcal{D} \subseteq \mathbb{R}^{n_1 \times \dots \times n_d}$, we have that the map $\mathbf{Q}(\mathbf{f}) = \mathbf{y} + \gamma \mathbf{W}(\mathbf{f})$ is a contraction with Lipschitz constant $\gamma L_{\mathbf{W}}$.*

Consider an Adams-Moulton linear multistep method in the form

$$\mathbf{f}_{k+1} - \Delta t \alpha \mathbf{G}(\mathbf{f}_{k+1}) = \mathbf{f}_k + \Delta t \sum_{j=0}^{s-1} \beta_j \mathbf{G}_{k-j}, \quad (\text{B.1})$$

where $\mathbf{G}_j = \mathbf{G}(\mathbf{f}_j)$. We can easily construct a contraction mapping whose fixed point is \mathbf{f}_{k+1} . To this end, simply define

$$\mathbf{Q}_k(\mathbf{f}) = \mathbf{f}_k + \Delta t \sum_{j=0}^{s-1} \beta_j \mathbf{G}_{k-j} + \Delta t \alpha \mathbf{G}(\mathbf{f}) \quad (\text{B.2})$$

and apply Lemma B1 with

$$\mathbf{y} = \mathbf{f}_{k+1} = \mathbf{f}_k + \Delta t \sum_{j=0}^{s-1} \beta_j \mathbf{G}_{k-j},$$

the coefficient $\gamma = \Delta t \alpha$, and the Lipschitz function $\mathbf{W} = \mathbf{G}$. To analyze stability of the Adams-Moulton method in the sense of Theorem 2.1 let $\hat{\mathbf{f}}_0, \dots, \hat{\mathbf{f}}_{s-1}$ and $\tilde{\mathbf{f}}_0, \dots, \tilde{\mathbf{f}}_{s-1}$ be two sets of initial conditions. By collecting like terms and dividing we obtain

$$\left\| \hat{\mathbf{f}}_s - \tilde{\mathbf{f}}_s \right\| \leq \frac{\left\| \hat{\mathbf{f}}_0 - \tilde{\mathbf{f}}_0 \right\| + \Delta t \sum_{j=0}^{s-1} |\beta_j| L_{\mathbf{G}} \left\| \hat{\mathbf{f}}_{s-j} - \tilde{\mathbf{f}}_{s-j} \right\|}{1 - \Delta t |\alpha| L_{\mathbf{G}}}. \quad (\text{B.3})$$

For every $\Delta t \leq 1/(2|\alpha|L_{\mathbf{G}})$, we have the stability condition

$$\left\| \hat{\mathbf{f}}_s - \tilde{\mathbf{f}}_s \right\| \leq \left\| \hat{\mathbf{f}}_0 - \tilde{\mathbf{f}}_0 \right\| + 2\Delta t |\alpha| L_{\mathbf{G}} \left\| \hat{\mathbf{f}}_0 - \tilde{\mathbf{f}}_0 \right\| + \Delta t \sum_{j=0}^{s-1} 2|\beta_j| L_{\mathbf{G}} \left\| \hat{\mathbf{f}}_{s-j} - \tilde{\mathbf{f}}_{s-j} \right\| \quad (\text{B.4})$$

To define the map $\tilde{\mathbf{Q}}_k$ for the application of Theorem 3.1, we consider the following choice of truncations

$$\tilde{\mathbf{Q}}_k(\mathbf{f}, e_1, e_2, \dots, e_{s+3}) = \mathfrak{T}_{r_{s+3}} \left(\mathfrak{T}_{r_{s+2}}(\mathbf{f}_k) + \Delta t \alpha \mathfrak{T}_{r_{s+1}}(\mathbf{G}(\mathbf{f})) + \Delta t \sum_{j=0}^{s-1} \beta_j \mathfrak{T}_{r_{j+1}}(\mathbf{G}_{k-j}) \right) \quad (\text{B.5})$$

where $\|\mathfrak{T}_{r_j}(\mathbf{g}) - \mathbf{g}\| \leq e_j$ for each $1 \leq j \leq s+3$. In order to guarantee that Theorem 3.1 may be applied, we require that

$$e_{s+3} + e_{s+2} + \frac{e_{s+1}}{\Delta t |\alpha|} + \sum_{j=1}^s \frac{e_j}{\Delta t |\beta_{j-1}|} = \varepsilon, \quad (\text{B.6})$$

which allows us to approximate \mathbf{Q}_k with up to ε error. We may now list the contraction mapping recurrences (36)-(38) which take the form

$$\mathbf{g}^{[j+1]} = \mathbf{f}_k + \Delta t \sum_{j=0}^{s-1} \beta_j \mathbf{G}_{k-j} + \Delta t \alpha \mathbf{G} \left(\mathbf{f}_{k+1}^{[j]} \right), \quad (\text{B.7})$$

$$\varepsilon_j = \frac{1 - \Delta t |\alpha| L_G}{c} \left\| \mathbf{g}^{[j+1]} - \mathbf{f}_{k+1}^{[j]} \right\|, \quad (\text{B.8})$$

$$\mathbf{f}_{k+1}^{[j+1]} = \mathfrak{T}_{\mathbf{r}_{s+3}} \left(\mathfrak{T}_{\mathbf{r}_{s+2}} (\mathbf{f}_k) + \Delta t \alpha \mathfrak{T}_{\mathbf{r}_{s+1}} \left(\mathbf{G} \left(\mathbf{f}_{k+1}^{[j+1]} \right) \right) + \Delta t \sum_{j=0}^{s-1} \beta_j \mathfrak{T}_{\mathbf{r}_{j+1}} (\mathbf{G}_{k-j}) \right). \quad (\text{B.9})$$

By Theorem 3.1, the local error of this recurrence is

$$\left\| \mathbf{f}(s\Delta t) - \mathbf{f}_s^{[j]} \right\| \leq K_s \Delta t^{s+2} + G_c (\Delta t |\alpha| L_G) \varepsilon_{\text{tol}}. \quad (\text{B.10})$$

Thus we require that there is a constant $B > 0$ so that $\varepsilon_{\text{tol}} < B \Delta t^{s+2}$. All subsequent optimizations and truncations which were outlined for the Euler and midpoint case analyzed in Section 3 also apply here.

References

- [1] S. M. Allen and J. W. Cahn. Ground state structures in ordered binary alloys with second neighbor interactions. *Acta Metall.*, 20(3):423–433, 1972.
- [2] S. M. Allen and J. W. Cahn. A correction to the ground state of FCC binary ordered alloys with first and second neighbor pairwise interactions. *Scripta Metallurgica*, 7(12):1261–1264, 1973.
- [3] W. Austin, G. Ballard, and T. G. Kolda. Parallel tensor compression for large-scale scientific data. In *IPDPS'16: Proceedings of the 30th IEEE International Parallel and Distributed Processing Symposium*, pages 912–922, May 2016.
- [4] M. Bachmayr, R. Schneider, and A. Uschmajew. Tensor networks and hierarchical tensors for the solution of high-dimensional partial differential equations. *Found. of Comput. Math.*, 16(6), 2016.
- [5] J. Baldeaux and M. Gnewuch. Optimal randomized multilevel algorithms for infinite-dimensional integration on function spaces with ANOVA-type decomposition. *SIAM J. Numer. Anal.*, 52(3):1128–1155, 2014.
- [6] V. Barthelmann, E. Novak, and K. Ritter. High dimensional polynomial interpolation on sparse grids. *Advances in Computational Mechanics*, 12:273–288, 2000.
- [7] M. J. Beran. *Statistical continuum theories*. New York: Interscience Publishers, 1968.
- [8] A. M. P. Boelens, D. Venturi, and D. M. Tartakovsky. Parallel tensor methods for high-dimensional linear PDEs. *J. Comput. Phys.*, 375:519–539, 2018.

- [9] A. M. P. Boelens, D. Venturi, and D. M. Tartakovsky. Tensor methods for the Boltzmann-BGK equation. *J. Comput. Phys.*, 421:109744, 2020.
- [10] H. J. Bungartz and M. Griebel. Sparse grids. *Acta Numerica*, 13:147–269, 2004.
- [11] Y. Cao, Z. Chen, and M. Gunzburger. ANOVA expansions and efficient sampling methods for parameter dependent nonlinear PDEs. *Int. J. Numer. Anal. Model.*, 6:256–273, 2009.
- [12] Y. Chen, L. Zhang, H. Wang, and W. E. Ground state energy functional with Hartree-Fock efficiency and chemical accuracy. *J. Phys. Chem. A*, 124(35), 2020.
- [13] H. Cho, D. Venturi, and G.E. Karniadakis. Numerical methods for high-dimensional probability density function equations. *J. Comput. Phys.*, 305:817–837, January 2016.
- [14] H. Al Daas, G. Ballard, and P. Benner. Parallel algorithms for tensor train arithmetic. *SIAM J. Sci. Comput.*, 44(1):C25–C53, 2022.
- [15] A. Dektor and D. Venturi. Dynamically orthogonal tensor methods for high-dimensional nonlinear PDEs. *J. Comput. Phys.*, 404:109125, 2020.
- [16] A. Dektor and D. Venturi. Dynamic tensor approximation of high-dimensional nonlinear PDEs. *J. Comput. Phys.*, 437:110295, 2021.
- [17] G. Di Marco and L. Pareschi. Numerical methods for kinetic equations. *Acta Numerica*, 23:369–520, May 2014.
- [18] S. Dolgov, B. Khoromskij, and I. Oseledets. Fast solution of parabolic problems in the tensor train/quantized tensor train format with initial application to the Fokker–Planck equation. *SIAM J. Sci. Comput.*, 34(6):A3016–A3038, 2012.
- [19] W. E, J. Han, and Q. Li. A mean-field optimal control formulation of deep learning. *Res. Math. Sci.*, 6(10):1–41, 2019.
- [20] J. Foo and G. E. Karniadakis. Multi-element probabilistic collocation method in high dimensions. *J. Comput. Phys.*, 229:1536–1557, 2010.
- [21] L. Grasedyck. Hierarchical singular value decomposition of tensors. *SIAM J. Matrix Anal. Appl.*, 31(4):2029–2054, 2010.
- [22] L. Grasedyck and C. Löbbert. Distributed hierarchical SVD in the hierarchical Tucker format. *Numer. Linear Algebra Appl.*, 25(6):e2174, 2018.
- [23] E. Hairer, C. Lubich, and G. Wanner. *Geometric numerical integration*, volume 31 of *Springer Series in Computational Mathematics*. Springer-Verlag, Berlin, second edition, 2006. Structure-preserving algorithms for ordinary differential equations.
- [24] E. Hairer, G. Wanner, and S. P. Nørsett. *Solving ordinary differential equations I: Nons-tiff problems*, volume 8 of *Springer Series in Computational Mathematics*,. Springer Berlin Heidelberg, second edition, 1993.
- [25] J. S. Hesthaven, S. Gottlieb, and D. Gottlieb. *Spectral methods for time-dependent problems*. Cambridge University Press, 2007.

- [26] E. Hopf. Statistical hydromechanics and functional calculus. *J. Rat. Mech. Anal.*, 1(1):87–123, 1952.
- [27] A.-K. Kassam and L. N. Trefethen. Fourth-order time stepping for stiff PDEs. *SIAM J. Sci. Comput.*, 26(4):1214–1233, 2005.
- [28] B. N. Khoromskij. Tensor numerical methods for multidimensional PDEs: theoretical analysis and initial applications. In *CEMRACS 2013—modelling and simulation of complex systems: stochastic and deterministic approaches*, volume 48 of *ESAIM Proc. Surveys*, pages 1–28. EDP Sci., Les Ulis, 2015.
- [29] E. Kieri and B. Vandereycken. Projection methods for dynamical low-rank approximation of high-dimensional problems. *Comput. Methods Appl. Math.*, 19(1):73–92, 2019.
- [30] D. Kressner and C. Tobler. Algorithm 941: htucker – a Matlab toolbox for tensors in hierarchical Tucker format. *ACM Transactions on Mathematical Software*, 40(3):1–22, 2014.
- [31] G. Li and H. Rabitz. Regularized random-sampling high dimensional model representation (RS-HDMR). *J. Math. Chem.*, 43(3):1207–1232, 2008.
- [32] H. Montanelli and Y. Nakatsukasa. Fourth-order time-stepping for stiff PDEs on the sphere. *SIAM J. Sci. Comput.*, 40(1):A421–A451, 2018.
- [33] A. Narayan and J. Jakeman. Adaptive Leja sparse grid constructions for stochastic collocation and high-dimensional approximation. *SIAM J. Sci. Comput.*, 36(6):A2952–A2983, 2014.
- [34] M. Raissi and G. E. Karniadakis. Hidden physics models: Machine learning of nonlinear partial differential equations. *J. Comput. Phys.*, 357:125–141, 2018.
- [35] M. Raissi, P. Perdikaris, and G. E. Karniadakis. Physics-informed neural networks: A deep learning framework for solving forward and inverse problems involving nonlinear partial differential equations. *J. Comput. Phys.*, 378:606–707, 2019.
- [36] H. Risken. *The Fokker-Planck equation: methods of solution and applications*. Springer-Verlag, second edition, 1989. Mathematics in science and engineering, vol. 60.
- [37] A. Rodgers, A. Dektor, and D. Venturi. Adaptive integration of nonlinear evolution equations on tensor manifolds. *J. Sci. Comput.*, 92(39):1–31, 2022.
- [38] A. Rodgers and D. Venturi. Stability analysis of hierarchical tensor methods for time-dependent PDEs. *J. Comput. Phys.*, 409:109341, 2020.
- [39] S. H. Rudy, S. L. Brunton, J. L. Proctor, and J. N. Kutz. Data-driven discovery of partial differential equations. *Science Adv.*, 3(4):e1602614, 2017.
- [40] T. Shi, M. Ruth, and A. Townsend. Parallel algorithms for computing the tensor-train decomposition. *ArXiv*, (2111.10448):1–23, 2021.
- [41] A. Trombettoni and A. Smerzi. Discrete solitons and breathers with dilute Bose-Einstein condensates. *Phys. Rev. Lett.*, 86:2353–2356, 2001.

- [42] A. Uschmajew. Local convergence of the alternating least squares algorithm for canonical tensor approximation. *SIAM J. Matrix Anal. Appl.*, 33(2):639–652, 2012.
- [43] A. Uschmajew and B. Vandereycken. The geometry of algorithms using hierarchical tensors. *Linear Algebra Appl.*, 439(1):133–166, 2013.
- [44] D. Venturi. The numerical approximation of nonlinear functionals and functional differential equations. *Phys. Reports*, 732:1–102, 2018.
- [45] D. Venturi and A. Dektor. Spectral methods for nonlinear functionals and functional differential equations. *Research in the Mathematical Sciences*, 8(27):1–39, 2021.
- [46] Y. Zhu, N. Zabaras, P.-S. Koutsourelakis, and P. Perdikaris. Physics-constrained deep learning for high-dimensional surrogate modeling and uncertainty quantification without labeled data. *J. Comput. Phys.*, 394:56–81, 2019.
- [47] J. Zinn-Justin. *Quantum field theory and critical phenomena*. Oxford Univ. Press, fourth edition, 2002.